Elsevier Editorial System(tm) for Applied Catalysis B: Environmental

Manuscript Draft

Manuscript Number: APCATB-D-18-00816R2

Title: On the promotional effect of Cu on Pt for hydrazine electrooxidation in alkaline medium

Article Type: Research Paper

Keywords: Direct Hydrazine Fuel Cells; Alkaline Media; Electrocatalysts; PtCu/C.

Corresponding Author: Mr. Jose Joaquin Joaquin Linares, Ph. D

Corresponding Author's Institution: Instituto de Química

First Author: Rudy Crisafulli, Doctor

Order of Authors: Rudy Crisafulli, Doctor; Vanine V Silva de Barros, Graduate; Francisca E Rodrigues de Oliveira, Master; Thairo de Araújo Rocha, Doctor; Sabrina Zignani, Doctor; Lorenzo Spadaro; Alessandra Palella; Jose A Dias, Doctor; Jose Joaquin Joaquin Linares, Ph. D

Brasília, April 30th, 2018.

Dear Editor of the Applied Catalysis B: Environmental,

Please find attached the revised version of manuscript "*On the promotional effect of Cu on Pt for hydrazine electrooxidation in alkaline medium*" by Rudy Crisafulli, Vanine V. Silva de Barros, Francisca E. Rodrigues de Oliveira, Thairo de Araújo Rocha, Sabrina Zignani, Lorenzo Spadaro, Alessandra Palella, José A. Dias, José J. Linares, to be submitted as an Original Research Article to *Applied Catalysis B: Environmental* for consideration of publication. We want to attest that this manuscript has not been previously published, and it is not under consideration by any other journal. All the authors are aware of, and accept responsibility for the whole content of the manuscript. The authors declare no competing financial interest.

In the revised version, the authors have changed the discussion of the fuel cell results (referred to Fig. 6) with respect to the comparison to other studies. We hope that this change will help the reader to better understand and contextualize the significance of this work in line with other recent works presented in the literature (references 57 and 58).

"*Figures 6a and 6b show the polarization curves, while Figs. 6c and 6d display the power density curves in a single DHFC operating at 60 and 80 °C, using* $Pt_{73}Cu_{27}/C$, $Pt_{53}Cu_{47}/C$, $Pt_{29}Cu_{71}/C$, *and Pt/C electrocatalysts as anodes. As can be observed, the polarization curves confirm that, regardless of the temperature, the* $Pt_{53}Cu_{47}/C$ *is the most active material with the highest current densities, as seen in the three-electrode glass cell. These results are also corroborated by the power densities at 60 and 80 ºC. Table 4 lists the maximum power densities (MPDs) and performance improvements (PIs) with respect to the Pt/C electrocatalyst, and it can be seen that the highest values were found for the* $Pt_{53}Cu_{47}/C$. *In this material, it is possible to achieve the maximum fraction of PtCu alloy with the optimum fraction of copper oxides present in the surface. The lower degree of alloying of the other two PtCu electrocatalysts and, particularly, the reduced amount of copper/copper oxides in the* $Pt_{73}Cu_{27}/C$ *explain the observed sequence* $Pt_{53}Cu_{47}/C > Pt_{29}Cu_{71}/C > Pt_{73}Cu_{27}/C > Pt/C$. *Finally, it is interesting to observe that the PI becomes stronger as the temperature increases. This could be explained by the activation of the Cu phase, which reinforces the auxiliary effects discussed extensively above. Thus, the potential to reduce noble metal loading in this application is consistent with other studies such as [57,58], which also show potential for high-performance DHFC technology utilizing either low- or non-noble metal electrocatalysts.*"

Looking forward to hearing from you soon.

Sincerely yours,

José Joaquín Linares León, on behalf of the authors.

Corresponding author:

Prof. José Joaquín Linares León

Laboratório de Desenvolvimento de Processos Químicos, Universidade de Brasília, Campus Universitário Darcy Ribeiro, 70910-900, Brasília, Distrito Federal, Brazil.

Email: joselinares@unb.br

CHANGES IN THE REVISED MANUSCRIPT APCATB-D-18-00816R1

Authors thank the suggestion given by the editor and, in order to better address the comment of reviewer 1 referring to adding references 57 and 58, has proceeded to correct the manuscript as follows (page 16 of the revised version of the manuscript). Authors hope that this modification is more suitable to highlight the relevance of this study and compare with the suggested references.

"*Figures 6a and 6b show the polarization curves, while Figs. 6c and 6d display the power density curves in a single DHFC operating at 60 and 80 °C, using* $Pt_{73}Cu_{27}/C$, $Pt_{53}Cu_{47}/C$, $Pt_{29}Cu_{71}/C$, *and Pt/C electrocatalysts as anodes. As can be observed, the polarization curves confirm that, regardless of the temperature, the* $Pt_{53}Cu_{47}/C$ *is the most active material with the highest current densities, as seen in the three-electrode glass cell. These results are also corroborated by the power densities at 60 and 80 ºC. Table 4 lists the maximum power densities (MPDs) and performance improvements (PIs) with respect to the Pt/C electrocatalyst, and it can be seen that the highest values were found for the* $Pt_{53}Cu_{47}/C$. *In this material, it is possible to achieve the maximum fraction of PtCu alloy with the optimum fraction of copper oxides present in the surface. The lower degree of alloying of the other two PtCu electrocatalysts and, particularly, the reduced amount of copper/copper oxides in the* $Pt_{73}Cu_{27}/C$ *explain the observed sequence* $Pt_{53}Cu_{47}/C$ > $Pt_{29}Cu_{71}/C$ > $Pt_{73}Cu_{27}/C$ > *Pt/C. Finally, it is interesting to observe that the PI becomes stronger as the temperature increases. This could be explained by the activation of the Cu phase, which reinforces the auxiliary effects discussed extensively above. Thus, the potential to reduce noble metal loading in this application is consistent with other studies such as [57,58], which also show potential for high-performance DHFC technology utilizing either low- or non-noble metal electrocatalysts.*"

On the promotional effect of Cu on Pt for hydrazine electrooxidation in alkaline medium

Rudy Crisafulli,[*1] Vanine V. Silva de Barros,[1] Francisca E. Rodrigues de Oliveira,[2] Thairo de Araújo Rocha,[2] Sabrina Zignani,[3] Lorenzo Spadaro,[3] Alessandra Palella,[3] José A. Dias,[4] José J. Linares[*1]

[1] Laboratório de Desenvolvimento de Processos Químicos, Universidade de Brasília, Campus Universitário Darcy Ribeiro, 70910-900 Brasília, Distrito Federal, Brazil

[2] Instituto de Química de São Carlos, Universidade de São Paulo, Av. Trabalhador São-Carlense, 400, 13566-590 São Carlos, SP, Brazil

[3] ITAE – Istituto di Tecnologie Avanzate per l'Energia "Nicola Giordano", Salita Santa Lucia Sopra Contesse, 5, 98126 Messina (ME), Italy

[4] Laboratório de Catálise, Instituto de Química, Universidade de Brasília, Campus Universitário Darcy Ribeiro, Brasília, DF, 70910-900, Brazil.

* Corresponding authors: José J. Linares (Tel.: +556131073828, Fax: +556132734149, Email: joselinares@unb.br); Rudy Crisafulli (Email: rudyunb@gmail.com).

ABSTRACT

Pt/C and PtCu/C electrocatalysts with nominal Pt:Cu atomic ratios of 75:25, 50:50, and 25:75 were prepared using N_2H_4 as reducing agent and carbon black Vulcan XC-72R as support. The obtained materials were physically characterized by X-ray diffraction, Energy-Dispersive X-ray analysis, Transmission Electron Microscopy images, X-ray Photoelectron Spectroscopy (XPS), and Temperature-Programmed Reduction analysis. Cyclic voltammetry, linear sweep voltammetry, and chronoamperometry (TPR) measurements were carried out in a three-electrode glass cell to evaluate the electrochemical activity towards hydrazine electrooxidation in alkaline medium along with single-cell direct hydrazine fuel cell (DHFC) tests. The actual composition of the electrocatalysts evidenced a slightly lower Cu fraction compared to the nominal one. The X-ray diffractograms of the electrocatalysts showed the typical face-centered cubic structure of Pt alloys, with the highest fraction of Cu alloyed to Pt being achieved with the almost equiatomic catalyst. An important fraction of the remaining non-alloyed Cu is in the form of a copper oxide, as evidenced by XPS and TPR measurements. The electrochemical tests evidenced that the coexistence of part of the Cu alloyed with Pt and copper oxide achieved in the PtCu/C electrocatalysts enhances the performance compared to Pt/C. In particular, the optimum formulation is attained by the $Pt_{53}Cu_{47}$/C electrocatalyst, allowing maximization of the electrocatalytic activity towards hydrazine electrooxidation and the single-cell performance at 60 and 80 °C.

Keywords: Direct Hydrazine Fuel Cells; Alkaline Media; Electrocatalysts; PtCu/C.

1. Introduction

Due to operational and infrastructure problems related to the use of hydrogen as fuel in proton exchange membrane fuel cells (PEMFCs) [1-3], liquid fuels have been proposed as an alternative. Their direct oxidation avoids the need to install an onboard reformate system, as proposed for the alcohols [4]. Within the group of liquid fuels, hydrazine appears as a promising candidate. Its synthesis is relatively simple and can be combined with the mass production of ammonia, resulting in a relatively economical fuel.

Hydrazine monohydrate [$N_2H_4 \cdot H_2O$, normal boiling point (NBP) = 121 °C] can be used directly as fuel in PEMFCs: it shows less volatility than the conventional alcohols used in fuel cells (methanol, NBP = 65 ºC; ethanol, NBP = 78 ºC), non-flammability, and a melting temperature of approximately –50 ºC, which makes its use in cold countries feasible [5]. According to the International Agency for Research on Cancer (IARC), hydrazine monohydrate is classified as 2B, like gasoline, so the safety protocols used for handling gasoline may be maintained for hydrazine monohydrate[5]. Furthermore, in Direct Hydrazine Fuel Cells (DHFCs), nitrogen and water are the final byproducts obtained. Furthermore, a high cell voltage with a potential maximum cell voltage of 1.62 V can theoretically be produced by hydrazine electrooxidation (HYEO) and oxygen electroreduction. DHFCs have been operated under acidic and alkaline conditions. In acidic medium, noble metals such as platinum and palladium are generally used [6]. In alkaline medium, other metals such as rhodium, ruthenium, gold, and silver and common metals such as copper also present electrocatalytic activity towards HYEO and have been tested with success in DHFCs [6,7]. Leading investigations have been presented by the Daihatsu Motor Company (Japan) in partnership with Prof. Atanassov's research group and Los Alamos National Laboratory (USA). They present promising electrochemical results accompanied by extensive

physico-chemical characterizations with Pt-free electrocatalysts based on Ni (NiMo/C [8] and $NiO/Nb_2O_5/C$ [9]) in the search for highly active and selective (minimizing the formation of NH_3) material. Furthermore, Sakamoto et al. [10] recently proposed a multi-step reaction DHFC, a promising alternative offering a stable power output over long operating periods. In this approach, both hydrazine and hydrogen (from the chemical decomposition of hydrazine) are used as fuel, allowing a significant reduction of the hydrazine crossover and the formation of radicals from the combination of hydrazine and oxygen in the cathode.

Platinum is considered as a reference material for HYEO. Compton and Aldous [11] showed that in the presence of activated or oxidized Pt, the Pt surface becomes more active, with a significant reduction in the onset potential. On the other hand, as mentioned above, copper, which is more abundant and affordable, is an active material for HYEO, especially in alkaline medium, in both the metallic [12-16] and oxidized forms [16-19]. Moreover, a very recent study presented by de Oliveira et al. [20] demonstrated the importance of the presence of oxidized sites (NiO_x) adjacent to Pt to promote the HYEO through a bifunctional effect. Furthermore, the formation of a PtCu alloy can also lead to changes in the Pt electronic environment that modify the binding energy of the reactants on the catalytic active sites (electronic effect) [21]. In this sense, Karaca et al. [22] have evidenced a significant enhancement when using a PtCu alloy for the hydrolytic dehydrogenation of ammonia and hydrazine borane. Therefore, the preparation of a PtCu electrocatalyst may be of interest for DHFCs if the bifunctional and electronic effects of the formation of the bimetallic alloy and the presence of copper oxides could be combined.

With this background, this paper shows the results of a study in which carbon-supported PtCu bimetallic electrocatalysts with different Pt:Cu atomic proportions have

been prepared by chemical reduction with hydrazine. The catalysts have been physically characterized by X-Ray Diffraction (XRD), Energy-Dispersive X-Ray (EDX) spectroscopy, Transmission Electron Microscopy (TEM), X-ray Photoelectron Spectroscopy (XPS), and Temperature-Programmed Reduction (TPR) to attain a complete description of the prepared materials. The physical and morphological information obtained is subsequently used to assist in interpreting the electrochemical activity for HYEO, which is evaluated by linear sweep voltammetry (LSV) and chronoamperometric studies (CA) in a three-electrode glass cell, and by application as anodes in an alkaline single-cell DHFC.

2. Experimental

Four electrocatalysts with a nominal metal loading of 20 wt.%, Pt, $Pt_{75}Cu_{25}C$, $Pt_{50}Cu_{50}$, and $Pt_{25}Cu_{75}$, deposited on carbon black (Vulcan XC-72R, Cabot Corp.), were prepared by chemical reduction with hydrazine (CRH, $N_2H_4 \cdot H_2O$, Sigma Aldrich). The chemicals $H_2PtCl_6.6H_2O$ (Aldrich) and $CuCl_2.2H_2O$ (Synth) were used as metal sources, while 2-propanol (Synth) and ultra-pure water (Milli-Q, Millipore) were used as solvents. For the preparation of 500 mg of electrocatalysts, the required metal salts were dissolved in 200 mL of a water/2-propanol (90/10 v/v) solution. Subsequently, 400 mg of the carbon support was added to solution and the resulting mixture was sonicated for 30 min. After this time had elapsed, the mixture was placed under vigorous stirring and a reducing solution (50 mL of 2:1 v/v of water/hydrazine) was added at once. The reaction medium was kept under stirring for 30 min at room temperature. Finally, the mixture was filtered and the obtained material was washed with excess water and dried at 70 °C for 2 h.

The Pt:Cu atomic ratios of the bulk of the electrocatalysts were obtained by EDX analysis using a JEOL 2100 scanning electron microscope with a 15-keV electron beam. The XRD analyses were carried out in a Rigaku model D8 Focus diffractometer using Cu K_α radiation (λ = 0.15406 nm). The diffractograms were recorded with 2θ angles in the range of 20 to 90° (0.05º step, 0.5º min^{-1}). The average crystallite (*d*) size was obtained by the application of Scherrer's equation (1), where *K* is a particle-shape-dependent constant (0.9 for spherical particles), λ is the wavelength of the incident radiation (Cu K_α), θ is the angle of the (*hkl*) peak, and $\beta_{(2\theta)}$ is the width in radians of the diffraction peak at half height.

$$d = \frac{K\lambda}{\beta_{(2\theta)} \cos\theta} \quad (1)$$

TEM analysis was performed using a JEOL 2100 microscope operating at 200 kV with point-to-point resolution of 0.19 Å. The particle size distribution was estimated from observations of at least 300 particles in different images. The average particle size, *D*, was calculated according to Equation 2, where n_i represents the number of particles of diameter D_i. The sample holder was composed of a gold grid covered by Lacey carbon (EMS).

$$D = \frac{\sum_i n_i D_i}{\sum_i n_i} \quad (2)$$

XPS measurements were carried out using a Physical Electronics (PHI) 5800-01 spectrometer. A monochromatic Al K_α X-ray source was used at a power of 350 W. Spectra were obtained with pass energies of 58.7 eV for elemental analysis and 11.75 eV for determination of the oxidation states. The pressure in the analysis chamber of the spectrometer was 10^{-9} torr during measurements. The Ag $3d_{5/2}$ peak of an Ag foil was used, after argon sputtering, to check the calibration of the binding energy scale.

Quantitative evaluation of each peak was performed by dividing the integrated peak area by atomic sensitivity factors, which were calculated from the ionization cross-sections, the mean free electron escape depth, and the measured transmission functions of the spectrometer. XPS data were interpreted by using the online library of oxidation states implemented in PHI MultiPak 6.1 software and the PHI *Handbook of X-ray Photoelectron Spectroscopy* [23]. By using this technique, it is possible to obtain information about the outermost layers of the metallic nanoparticles, which are fundamental for the electrocatalytic activity [24].

The TPR profiles were obtained under hydrogen atmosphere in a linear quartz microreactor (i.d. = 4 mm) fed with a 5-vol.% H_2/Ar purified carrier at a rate of 30 sccm. The experiments were carried out in the range of 25 to 900 °C at a heating rate of 10 °C min^{-1}. The weight of sample used was approximately 15 mg. The hydrogen consumption was monitored by a thermal conductivity detector calibrated against the peak area of known amounts of CuO. The resultant TPR data were highly reproducible in terms of the positions of maxima (± 2 °C) and extent of H_2 consumption (± 3 °C).

Electrochemical studies were carried out using the ultra-thin coating technique. Electrochemical measurements were performed in a three-electrode cell using a platinized Pt plate as counter electrode, an Hg/HgO/KOH electrode as reference electrode, and a reticulated vitreous carbon (RVC) working electrode (5 mm in diameter). This electrode was prepared by dispersing 1 mg of the electrocatalysts in 1 mL of 2-propanol. The mixture was sonicated for 10 min; then, with the aid of a chromatographic syringe, 20 μL of the dispersion was transferred onto the surface of the previously polished RVC electrode. The experiments were performed using a μ-Autolab (model Type III) potentiostat/galvanostat coupled to a personal computer and General Purpose Electrochemical System (GPES) software. CV measurements were performed

in a 1.0 mol L^{-1} KOH solution at a scan rate of 10 mV s^{-1}. The study of HYEO was performed at room temperature by LSV and chronoamperometry (for 30 min) at 0.024 V versus Hg/HgO in a solution of 1.0 mol L^{-1} hydrazine in 1.0 mol L^{-1} KOH. The current values obtained were Pt-mass normalized.

DHFC tests were performed on a single cell. Electrodes with an active area of 4 cm^2 were prepared as follows. For the anodes, a catalytic ink containing Pt/C or PtCu/C electrocatalyst (catalyst loading of 0.5 mg Pt cm^{-2} for both monometallic and bimetallic materials) and Nafion® emulsion [5 wt.% emulsion in a mixture of aliphatic alcohols (IonPower), forming 10 wt.% of the total catalyst] was brush-painted onto a carbon cloth (Zoltec PX30) diffusion layer. In a similar way, cathodes were prepared using 20 wt.% Pt/C (BASF fuel cells) using a Pt loading of 1 mg cm^{-2}. The membrane electrode assemblies were prepared by hot pressing the anode and cathode onto a pretreated Tokuyama membrane (24 h in 1 mol L^{-1} KOH solution) at 60 °C for 3 min under a pressure of 40.8 kg_f cm^{-2}. Electrical performances were determined from polarization and power density curves using a single cell at 60 and 80 °C. The fuel was delivered at 2.4 mL min^{-1} through the anode and pure oxygen flow was regulated at 30 sccm for the cathode.

3. Results and discussion

In order to assess the actual Pt:Cu ratios in the electrocatalysts, EDX analyses were carried out. Table 1 lists the corresponding results. In general, the obtained Pt:Cu atomic ratios were similar to the nominal values, with the exception of the electrocatalysts with the highest Cu fraction (Pt:Cu ratio of 25:75), where a higher Pt fraction of 29:71 was obtained. A possible reason for this will be discussed later on, based on the smaller fraction of Cu alloyed to Pt and greater presence of copper oxides,

whose anchorage on the carbon support is partially limited. This could also explain the higher deviation of the metallic content of the catalyst on the carbon support with respect to the nominal 20%; that is, the higher the Cu fraction, the greater the deviation. From now on, the electrocatalysts will be referred to by the actual compositions.

Insert Table 1 near here

Figure 1 shows the X-ray diffractograms of the Pt/C and PtCu/C electrocatalysts. As can be seen, all the diffractograms show a broad peak at about 25°, associated to the (200) facet of the hexagonal graphite structure, and five diffraction peaks at approximate angles of 40, 47, 67, 82, and 87°, associated to the (111), (200), (220), (311), and (222) facets, respectively, of Pt face-centered cubic (FCC) crystalline structure [25]. The (111) reflections of Pt crystalline structure were used to calculate the average crystallite sizes, whose values are listed in Table 2. All the prepared materials present crystallite sizes in the nanometric range (2–4 nm). However, the monometallic Pt/C catalyst shows a higher crystal size than the bimetallic materials. Hence during the formation of the crystallites, Cu (or copper oxide) exerts a protective role, leading to a smaller growth of the embryos formed during the drastic reduction induced by the hydrazine. The diffractograms also evidenced a shift of the peaks relative to Pt (FCC) phase to higher angles compared to those of the Pt/C electrocatalyst, indicating the formation of PtCu alloy [26,27]. Vegard's law can be applied to the PtCu bimetallic system [27-30] according to Equation 3, where a_{PtCu} represents the lattice parameter of the bimetallic material, a_{Pt} the lattice parameter of Pt (0.3912 nm), a_{Cu} the lattice parameter of Cu (0.3601 nm), and x_{Cu} the Cu fraction in the PtCu alloy.

$$a_{PtCu} = x_{Cu} a_{Cu} + (1 - x_{Cu}) a_{Pt} \quad (3)$$

From Equation 2, the Cu fraction in the alloy can be estimated along with the percentage of deposited Cu that is actually alloyed with Pt. For this purpose, Equation 4 must be applied, where $Cu_{alloyed}$ is the amount of Cu in the alloy as a percentage of the total amount of Cu, x is the fraction of copper in the $Pt_{1-x}Cu_x$ alloy, and Cu/Pt is the actual atomic ratio between the two metals.

$$Cu_{alloyed} = \frac{x_{Cu}}{(1 - x_{Cu})\left(Cu/Pt\right)} \quad (4)$$

The corresponding Cu fraction in the alloy and percentage of Cu alloyed are listed in Table 2. As observed, the Cu fraction in the PtCu alloy increases in the sequence from $Pt_{73}Cu_{27}$ to $Pt_{53}Cu_{47}$. The larger fraction of Cu in the catalyst formulation favors a higher Cu insertion in the Pt FCC structure. Oppositely, the $Pt_{29}Cu_{71}$/C shows a decrease in the degree of alloying. A possible explanation for this may be the catalytic role that Pt could play in favoring the Cu(II) reduction and incorporation in the alloy [31]. Indeed, a large fraction of non-alloyed Cu [segregated amorphous metal or copper (I and/or II) oxides] is present in the $Pt_{29}Cu_{71}$/C catalyst. In the other two formulations, the fraction of alloyed Cu remains almost the same, corroborating the important role of the Pt nuclei in forming the PtCu alloy. Higher fractions of alloyed Cu may be achieved by using other reducing agents such as borohydride or by studying the influence of the reduction conditions such as the temperature, reduction time, and/or reducing agent concentration, among others. Moreover, alternative reduction routes, such as the thermal one, may be promising.

Insert Figure 1 near here

Insert Table 2 near here

Figure 2 shows the TEM images of the different electrocatalysts and the corresponding particle size distribution. The average particle sizes are listed in Table 2. As can be observed, although the crystallite domains estimated by XRD are small, they tend to agglomerate, forming larger nanoparticles that are clearly visible in all the materials, leading to average particle sizes between 6 and 8 nm. Furthermore, the size distribution is rather heterogenous (from 2 to 18–20 nm), although small particles can be seen in the high-resolution image obtained for the $Pt_{53}Cu_{47}$/C (2–4 nm, Fig. 2e). The use of a strong reducing agent such as hydrazine may be responsible for these results, which suggests that a capping agent would be necessary to prepare electrocatalysts with a more homogeneous particle size distribution when using the strong reducing agent hydrazine.

Insert Figure 2 near here

The surface composition and oxidation state of platinum and copper on the surface of the $Pt_{73}Cu_{27}$/C, $Pt_{53}Cu_{47}$/C, and $Pt_{29}Cu_{71}$/C electrocatalysts were investigated using XPS. The respective spectra are displayed in Figure 3 and the estimated Pt and Cu percentages in the surface are listed in Table 3. The Pt 4f XPS spectra show the Pt $4f_{7/2}$ and Pt $4f_{5/2}$ peaks for metallic platinum at approximately 71.3 and 74.7 eV, respectively. The Pt spectra also display three peaks at approximately 72.5, 75.5, and 77.4 eV, associated with electronic transitions of 4f electrons of PtO, $Pt(OH)_2$, and PtO_2 species [32-34]. One interesting feature observed in the Pt 4f spectra is the appearance of a more intense signal in the region of highest energy (78–82 eV), where the Cu fraction is higher. A tentative assignment would be the Cu $3p_{1/2}$ signal of the copper oxide [35], in consonance with the greater presence of this species. An estimation of the ratio of metallic to oxidized Pt reveals that the amount of metallic Pt remains almost constant in

the $Pt_{73}Cu_{27}$/C and $Pt_{53}Cu_{47}$/C, whereas Pt oxide species are predominant in the $Pt_{29}Cu_{71}$/C, in which the presence of a larger amount of copper oxides species may induce the formation of surface PtO_x sites. Finally, a very interesting feature observed in the Pt 4f spectra is the downshift of the Pt $4f_{7/2}$ (71.4 eV for $Pt_{73}Cu_{27}$/C, 71.1 eV for $Pt_{53}Cu_{47}$/C, and 71.5 eV for $Pt_{29}Cu_{71}$/C) for the most alloyed electrocatalysts, evidencing an electronic effect of Cu on the sites of the outermost Pt layers. Regarding the Cu 2p spectra, $Pt_{73}Cu_{27}$/C shows tiny peaks at approximately 932 and 952 eV, attributed to metallic copper or cuprous oxide, along with a weak satellite signal ascribed to the presence of small amounts of cupric oxide [27,28,36,37]. These peaks become more evident in the $Pt_{53}Cu_{47}$/C material, at 934 and 954 eV, in addition to the satellites at 943 and 963 eV. The strongest evidences of the presence of CuO are observable in the $Pt_{29}Cu_{71}$/C. Hence, the higher the fraction of Cu, the larger the tendency to form copper oxide species, whose presence may induce the larger fraction of surface Pt oxides.

Insert Figure 3 near here

Insert Table 3 near here

Table 3 also lists the Pt:Cu surface composition. As can be seen, a comparison between the actual ratio of metals and the surface one reveals a certain enrichment of Pt. This result may be explained in terms of a possible galvanic displacement of the nanometallic copper nanoparticles formed during the reduction process by the Pt precursor [38]. Metallic copper then transforms into Cu(II) species. The higher the Cu content in the catalyst formulation, the more severe this phenomenon would be, which could explain the more prominent CuO peaks observed in the XPS spectra. Furthermore, soluble Cu^{2+} could be formed, which would support the reduction of the

metallic content observed in the EDX results at a higher Cu fraction in the catalyst formulation and greater Pt enrichment in the catalyst surface.

Figure 4 shows the TPR signals of the $Pt_{73}Cu_{27}$/C, $Pt_{53}Cu_{47}$/C, and $Pt_{29}Cu_{71}$/C electrocatalysts. As can be observed, all the materials present an initial reduction peak (peak 1) at low temperature (60–80 °C). This temperature relatively low compared to others reported in the literature for Pt/C catalysts (in the range of 100–200 °C [39-42]). This peak is attributed to the reduction of surface platinum oxides. Subsequently, a larger peak (peak 2) appears in the range of 180 to 210 °C for all the materials. This peak can be ascribed to the mixed reduction of both metals in the PtCu alloy [43,44]. Furthermore, this peak can contain a contribution from copper oxides, which are reduced at lower temperature (approx. 200 °C) in the presence of Pt [41]. Furthermore, the most alloyed electrocatalyst possesses the lowest temperature for the maximum in the signal compared to the other catalysts, corroborating that the Pt can exert a spillover effect on copper oxides. The third and fourth peaks in the first low-temperature region of the TPR profiles appear in the ranges of 290–310 °C and 440–460 °C in the $Pt_{73}Cu_{27}$/C and $Pt_{53}Cu_{47}$/C catalysts. According to the literature [43] (and in agreement with the XPS spectra), those peaks may be assigned to the reduction of Cu_2O and CuO species that are not interacting with Pt. It is interesting to note that in the $Pt_{53}Cu_{47}$/C, the area of the peaks is larger (a larger Cu fraction), although their proportions are similar. Thus it can be speculated that, in percentage terms, the copper speciation is similar in both materials. Finally, two large peaks can be observed above 500 °C (peaks 5 and 6 of $Pt_{73}Cu_{27}$/C and $Pt_{53}Cu_{47}$/C). These can be ascribed to gasification of the carbon support [39], even though large Cu_2O/CuO particle sizes may also contribute to the lowest temperature peak [45]. In the case of the $Pt_{29}Cu_{71}$/C, a very weak peak can be identified at 268 °C (peak 3) and is tentatively assigned to a small amount of cuprous oxide. The

fourth peak, centered at 552 °C, may contain a simultaneous contribution from the predominant cupric oxide and support gasification. The final peak (peak 5, > 650 °C) is assigned to gasification of the carbon support. A very interesting feature of the TPR profiles is the increase observed in the TCD signal as the Cu fraction in the electrocatalysts increases, with special significance in the case of the $Pt_{29}Cu_{71}$/C, confirming the larger amount of oxidized species deposited on the carbon support.

Insert Figure 4 near here

Figure 5a displays the corresponding cyclic voltammograms in alkaline medium (1 mol L^{-1} KOH) of Pt/C and the PtCu/C electrocatalysts. As can be seen, the profiles of the PtCu/C electrocatalysts do not show the characteristic anodic stripping peaks associated with the hydrogen adsorption/desorption on Pt surface atoms (–0.8 to –0.5 V vs. Hg/HgO) typical of Pt/C. This is a consequence of inhibition of the hydrogen adsorption/oxidation processes over Pt and can be attributed to the incorporation of copper within the structure of platinum on the PtCu/C electrocatalyst surfaces [46]. Also, the PtCu/C electrocatalysts show an increase in the currents in the double layer (–0.55 and 0.3 V vs. Hg/HgO) with increasing copper content, which is ascribed to the growing presence of copper oxides [47-49]. Finally, larger currents are observed in the regions of Pt-oxide formation/reduction, whose intensification is due to important contributions from copper redox pairs [50]. This feature becomes more evident at the higher Cu fraction as a result of the more Cu-enriched surface.

The electrochemical activity towards HYEO is assessed by LSV. Figure 5b displays the corresponding profiles. As can be observed, the HYEO activity improves notably when Cu is added to the catalyst formulation. In the literature [51,52], the formation of a PtCu alloy leads to a reduction of the unfilled Pt 5d states, lowering the adsorption strengths (of the eventual adsorbates formed) compared to Pt [53] and

diminishing the tendency to form platinum oxide at high potential. Two pieces of evidence can support this statement: the lower binding energy observed for the $Pt_{57}Cu_{47}/C$ in the Pt $4f_{7/2}$ region of the XPS spectra and the lower reduction temperature of Pt oxide species in the bimetallic materials. These features are indeed important. According to the literature [20], non-oxidized Pt sites are required for complete HYEO, where dissociative adsorption [20,54-56] takes place in order to produce adsorbed $N_2H_{x,ads}$ and H_{ads} species that are subsequently oxidized by adsorbed OH_{ads} and/or OH^-. The lower tendency to form Pt oxides in the alloyed PtCu along with the expected weaker adsorption strength can intrinsically accelerate the HYEO dissociative adsorption steps on Pt (electronic effect). On the other hand, the presence of oxidized copper species may contribute, through the bifunctional mechanism, by providing OH_{ads} species after OH^- discharge. Finally, copper/copper oxide species are active for HYEO, as stated in the Introduction. The combination of all these factors explains the enhanced electrochemical performance of the PtCu electrocatalysts. Regarding the composition, the most adequate (balanced) material is the almost equiatomic $Pt_{53}Cu_{47}/C$, in which almost half of the copper forms, with Pt, the most alloyed electrocatalyst in combination with an optimum amount of surface copper/copper oxides. In the $Pt_{73}Cu_{27}/C$, the lower degree of alloying attained and the reduced presence of copper diminish the electrochemical performance. The $Pt_{29}Cu_{71}/C$ also presents a lower degree of alloying and a high fraction of Cu species on the catalytic surface, limiting its performance. The presence of the active copper phase may reduce the size of the observed performance drop compared to $Pt_{73}Cu_{27}/C$. The chronoamperometric curves shown in Figure 5c confirm these results.

Insert Figure 5 near here

Insert Table 3 near here

Figures 6a and 6b show the polarization curves, while Figs. 6c and 6d display the power density curves in a single DHFC operating at 60 and 80 °C, using $Pt_{73}Cu_{27}$/C, $Pt_{53}Cu_{47}$/C, $Pt_{29}Cu_{71}$/C, and Pt/C electrocatalysts as anodes. As can be observed, the polarization curves confirm that, regardless of the temperature, the $Pt_{53}Cu_{47}$/C is the most active material with the highest current densities, as seen in the three-electrode glass cell. These results are also corroborated by the power densities at 60 and 80 ºC. Table 4 lists the maximum power densities (MPDs) and performance improvements (PIs) with respect to the Pt/C electrocatalyst, and it can be seen that the highest values were found for the $Pt_{53}Cu_{47}$/C. In this material, it is possible to achieve the maximum fraction of PtCu alloy with the optimum fraction of copper oxides present in the surface. The lower degree of alloying of the other two PtCu electrocatalysts and, particularly, the reduced amount of copper/copper oxides in the $Pt_{73}Cu_{27}$/C explain the observed sequence $Pt_{53}Cu_{47}$/C > $Pt_{29}Cu_{71}$/C > $Pt_{73}Cu_{27}$/C > Pt/C. Finally, it is interesting to observe that the PI becomes stronger as the temperature increases. This could be explained by the activation of the Cu phase, which reinforces the auxiliary effects discussed extensively above. Thus, the potential to reduce noble metal loading in this application is consistent with other studies such as [57,58], which also show potential for high-performance DHFC technology utilizing either low- or non-noble metal electrocatalysts.

Insert Figure 6 near here

Insert Table 4 near here

4. Conclusions

This study demonstrates the promotional effect of copper on the electrocatalytic activity for HYEO of platinum. The formation of a PtCu alloy seems to alter the electronic

environment favorably and is balanced by the presence of Cu oxide species that can donate OH_{ads} for completion of the HYEO, leading to a very active material for application in DHFCs. Despite some particle agglomeration due to the use of hydrazine as a strong reducing agent, the different highly electroactive Pt_xCu_{100-x}/C electrocatalysts outperform the reference Pt/C (also prepared by CRH). Regarding the Pt:Cu ratio, the highest performance is achieved with the almost equiatomic $Pt_{53}Cu_{47}/C$, whose electrocatalytic surface attains an optimum equilibrium between the largest fraction of Cu alloyed with Pt and the presence of active copper oxides. A lower Cu content in the catalyst formulation reduces the degree of alloying and especially the fraction of copper oxides. A higher Cu content also reduces the degree of alloying in these materials prepared by CRH, reducing the electronic effect despite the larger fraction of copper oxides. In this scenario, the electrochemical performances studied in a more fundamental glass cell and in an actual single DHFC lead to the following sequence of electroactive materials for HYEO: $Pt_{53}Cu_{47}/C > Pt_{29}Cu_{71}/C > Pt_{73}Cu_{27}/C >$ Pt/C.

Acknowledgments

The authors thank Coordenação de Aperfeiçoamento de Pessoal de Nível Superior (CAPES) for a scholarship awarded to Rudy Crisafulli. In addition, we acknowledge the research scholarship provided by CNPq and financial support provided by UnB/DPI/IQ, MCTI/CNPq, CAPES, FAP-DF, and FINEP/CTPetro.

References

[1] R. Moliner, M.J. Lazaro, I. Suelves, Analysis of the strategies for bridging the gap towards the hydrogen economy, Int. J. Hydrog. Energy 41 (2016) 19500–

19508. doi:10.1016/j.ijhydene.2016.06.202.

[2] M. Ball, M. Weeda, The hydrogen economy—Vision or reality? Int. J. Hydrog. Energy 40 (2015) 7903–7919. doi:10.1016/j.ijhydene.2015.04.032.

[3] R.M. Antoniassi, J.C.M. Silva, A. Oliveira Neto, E. V Spinacé, Synthesis of Pt+SnO2/C electrocatalysts containing Pt nanoparticles with preferential (100) orientation for direct ethanol fuel cell, Appl. Catal. B Environ. 218 (2017) 91–100. doi:10.1016/j.apcatb.2017.06.031.

[4] L. An, T.S. Zhao, S.Y. Shen, Q.X. Wu, R. Chen, Performance of a direct ethylene glycol fuel cell with an anion-exchange membrane, Int. J. Hydrog. Energy 35 (2010) 4329–4335. doi:10.1016/j.ijhydene.2010.02.009.

[5] T. Sakamoto, K. Asazawa, U. Martinez, B. Halevi, T. Suzuki, S. Arai, D. Matsumura, Y. Nishihata, P. Atanassov, H. Tanaka, Electrooxidation of hydrazine hydrate using Ni-La catalyst for anion exchange membrane fuel cells, J. Power Sources 234 (2013) 252–259. doi:10.1016/j.jpowsour.2013.01.181.

[6] A. Serov, C. Kwak, Direct hydrazine fuel cells: A review, Appl. Catal. B Environ. 98 (2010) 1–9. doi:10.1016/j.apcatb.2010.05.005.

[7] D.A. Finkelstein, R. Imbeault, S. Garbarino, L. Roué, D. Guay, Trends in catalysis and catalyst cost effectiveness for N2H4 fuel cells and sensors: a rotating disk electrode (RDE) study, J. Phys. Chem. C. 120 (2016) 4717–4738. doi:10.1021/acs.jpcc.5b10156.

[8] T. Asset, A. Roy, T. Sakamoto, M. Padilla, I. Matanovic, K. Artyushkova, A. Serov, F. Maillard, M. Chatenet, K. Asazawa, H. Tanaka, P. Atanassov, Highly active and selective nickel molybdenum catalysts for direct hydrazine fuel cell, Electrochim. Acta. 215 (2016) 420–426. doi:10.1016/j.electacta.2016.08.106.

[9] T. Sakamoto, T. Masuda, K. Yoshimoto, H. Kishi, S. Yamaguchi, D. Matsumura, K. Tamura, A. Hori, Y. Horiuchi, A. Serov, K. Artyushkova, P. Atanassov, H. Tanaka, NiO/Nb2O5/C hydrazine electrooxidation catalysts for anion exchange membrane fuel cells, J. Electrochem. Soc. 164 (2017) F229–F234. doi:10.1149/2.0281704jes.

[10] T. Sakamoto, A. Serov, T. Masuda, M. Kamakura, K. Yoshimoto, T. Omata, H. Kishi, S. Yamaguchi, A. Hori, Y. Horiuchi, T. Terada, K. Artyushkova, P. Atanassov, H. Tanaka, Highly durable direct hydrazine hydrate anion exchange membrane fuel cell, J. Power Sources 375 (2018) 291–299. doi:10.1016/j.jpowsour.2017.05.052.

[11] L. Aldous, R.G. Compton, The mechanism of hydrazine electro-oxidation revealed by platinum microelectrodes: role of residual oxides, Phys. Chem. Chem. Phys. 13 (2011) 5279–5287. doi:10.1039/C0CP02261F.

[12] F. Jia, J. Zhao, X. Yu, Nanoporous Cu film/Cu plate with superior catalytic performance toward electro-oxidation of hydrazine, J. Power Sources 222 (2013) 135–139. doi:10.1016/j.jpowsour.2012.08.076.

[13] E. Granot, B. Filanovsky, I. Presman, I. Kuras, F. Patolsky, Hydrazine / air direct-liquid fuel cell based on nanostructured copper anodes, J. Power Sources 204 (2012) 116–121. doi:10.1016/j.jpowsour.2011.12.008.

[14] S. Lal, M. Deepa, V.M. Janardhanan, K.C. Sahu, Paper based hydrazine monohydrate fuel cells with Cu and C composite catalysts, Electrochim. Acta.

232 (2017) 262–270. doi:10.1016/j.electacta.2017.02.118.

[15] H. Gao, Y. Wang, F. Xiao, C.B. Ching, H. Duan, Growth of copper nanocubes on graphene paper as free-standing electrodes for direct hydrazine fuel cells, J. Phys. Chem. C. 116 (2012) 7719–7725. doi:10.1021/jp3021276.

[16] G. Karim-Nezhad, R. Jafarloo, P.S. Dorraji, Copper (hydr)oxide modified copper electrode for electrocatalytic oxidation of hydrazine in alkaline media, Electrochim. Acta. 54 (2009) 5721–5726. doi:10.1016/j.electacta.2009.05.019.

[17] Y. Ma, H. Li, R. Wang, H. Wang, W. Lv, S. Ji, Ultrathin willow-like CuO nanoflakes as an efficient catalyst for electro-oxidation of hydrazine, J. Power Sources 289 (2015) 22–25. doi:10.1016/j.jpowsour.2015.04.151.

[18] S.R. Hosseini, M. Kamali-Rousta, Preparation of electro-spun CuO nanoparticle and its application for hydrazine hydrate electro-oxidation, Electrochim. Acta. 189 (2016) 45–53. doi:10.1016/j.electacta.2015.12.070.

[19] R.A. Soomro, Q. Baloach, A. Tahira, Z.H. Ibupoto, G.Q. Khaskheli, Sirajuddin, V.K. Deewani, K.R. Hallam, K. Rajar, M. Willander, Rice-like CuO nanostructures for sensitive electrochemical sensing of hydrazine, Microsyst. Technol. 23 (2017) 731–738. doi:10.1007/s00542-015-2726-x.

[20] D.C. de Oliveira, W.O. Silva, M. Chatenet, F.H.B.B. Lima, NiOx-Pt/C nanocomposites: Highly active electrocatalysts for the electrochemical oxidation of hydrazine, Appl. Catal. B Environ. 201 (2017) 22–28. doi:10.1016/j.apcatb.2016.08.007.

[21] S. Mukerjee, S. Srinivasan, M.P. Soriaga, J. McBreen, Role of structural and electronic properties of Pt and Pt alloys on electrocatalysis of oxygen reduction: an in situ XANES and EXAFS investigation, J. Electrochem. Soc. 142 (1995) 1409–1422. doi:10.1149/1.2048590.

[22] T. Karaca, M. Sevim, Ö. Metin, Facile synthesis of monodisperse copper–platinum alloy nanoparticles and their superb catalysis in the hydrolytic dehydrogenation of ammonia borane and hydrazine borane, ChemCatChem. 9 (2017) 4185–4190. doi:10.1002/cctc.201701023.

[23] J.F. Moulder, W.F. Stickle, P.E. Sobol, K.D. Bomben, Handbook of X-ray Photoelectron Spectroscopy, 1st ed., Perkin-Elmer Corporation, 1992.

[24] S. Liao, B. Li, Y. Li, Physical characterization of electrocatalysts, in: J. Zhang (Ed.), PEM Fuel Cell Electrocatalysts and Catalyst Layers: Fundamentals and Applications, Springer London, London, 2008, pp. 487–546. doi:10.1007/978-1-84800-936-3_10.

[25] J.W. Edwards, R. Speiser, H.L. Johnston, High temperature structure and thermal expansion of some metals as determined by X-Ray diffraction data. I. Platinum, tantalum, niobium, and molybdenum, J. Appl. Phys. 22 (1951) 424–428. doi:10.1063/1.1699977.

[26] W.J. Zhou, S.Q. Song, W.Z. Li, G.Q. Sun, Q. Xin, S. Kontou, K. Poulianitis, P. Tsiakaras, Pt-based anode catalysts for direct ethanol fuel cells, Solid State Ion. 175 (2004) 797–803. doi:10.1016/j.ssi.2004.09.055.

[27] E.A. Carbonio, F. Colmati, E.G. Ciapina, M.E. Pereira, E.R. Gonzalez, Pt-Cu/C and Pd Modified Pt-Cu/C electrocatalysts for the oxygen reduction reaction in

direct methanol fuel cells, J. Braz. Chem. Soc. 21 (2010) 590–602. doi: 10.1590/S0103-50532010000400003.

[28] E. Taylor, Synthesis of platinum and platinum-copper branched nanoparticles for electrooxidation of methanol, University of Arkansas, 2013. http://scholarworks.uark.edu/etd (accessed January 17, 2018).

[29] M. Millán, H. Zamora, M.A. Rodrigo, J. Lobato, Enhancement of electrode stability using platinum–cobalt nanocrystals on a novel composite SiCTiC support, ACS Appl. Mater. Interfaces 9 (2017) 5927–5936. doi:10.1021/acsami.6b13071.

[30] J. Lobato, P. Cañizares, M.A. Rodrigo, J.J. Linares, Study of different bimetallic anodic catalysts supported on carbon for a high temperature polybenzimidazole-based direct ethanol fuel cell, Appl. Catal. B Environ. 91 (2009) 269–274. doi:10.1016/j.apcatb.2009.05.035.

[31] M. Gong, Z. Yao, F. Lai, Y. Chen, Y. Tang, Platinum–copper alloy nanocrystals supported on reduced graphene oxide: One-pot synthesis and electrocatalytic applications, Carbon 91 (2015) 338–345. doi:10.1016/j.carbon.2015.05.006.

[32] K. Zhang, Q. Yue, G. Chen, Y. Zhai, L. Wang, H. Wang, J. Zhao, J. Liu, J. Jia, H. Li, Effects of acid treatment of Pt−Ni alloy nanoparticles@graphene on the kinetics of the oxygen reduction reaction in acidic and alkaline solutions, J. Phys. Chem. C. 115 (2011) 379–389. doi:10.1021/jp108305v.

[33] F. Papa, C. Negrila, G. Dobrescu, A. Miyazaki, I. Balint, Preparation, characterization and catalytic behavior of Pt-Cu nanoparticles in methane combustion, J. Nat. Gas Chem. 20 (2011) 537–542. doi:10.1016/S1003-9953(10)60221-6.

[34] S. Fu, C. Zhu, Q. Shi, D. Du, Y. Lin, Enhanced electrocatalytic activities of three dimensional PtCu@Pt bimetallic alloy nanofoams for oxygen reduction reaction, Catal. Sci. Technol. 6 (2016) 5052–5059. doi:10.1039/C5CY02288F.

[35] X. Du, S. Luo, H. Du, M. Tang, X. Huang, P.K. Shen, Monodisperse and self-assembled Pt-Cu nanoparticles as an efficient electrocatalyst for the methanol oxidation reaction, J. Mater. Chem. A. 4 (2016) 1579–1585. doi:10.1039/C5TA09261B.

[36] J.M. Machefert, A. D'Huysser, M. Lenglet, J. Lopitaux, D. Delahaye, Initial stage of copper thermal oxidation studied by UV-vis-NIR reflectance spectroscopy, XPS and X-ray diffraction, Mater. Res. Bull. 23 (1988) 1379–1388. doi:10.1016/0025-5408(88)90262-0.

[37] T.H. Fleisch, G.J. Mains, Reduction of copper oxides by UV radiation and atomic hydrogen studied by XPS, Appl. Surf. Sci. 10 (1982) 51–62. doi:10.1016/0378-5963(82)90134-9.

[38] A. Sarkar, A. Manthiram, Synthesis of Pt@Cu core−shell nanoparticles by galvanic displacement of Cu by Pt4+ ions and their application as electrocatalysts for oxygen reduction reaction in fuel cells, J. Phys. Chem. C. 114 (2010) 4725–4732. doi:10.1021/jp908933r.

[39] A. Ciftci, D.A.J.M. Ligthart, E.J.M. Hensen, Aqueous phase reforming of glycerol over Re-promoted Pt and Rh catalysts, Green Chem. 16 (2014) 853–863. doi:10.1039/C3GC42046A.

[40] F. Bossola, X.I. Pereira-Hernández, C. Evangelisti, Y. Wang, V. Dal Santo, Investigation of the promoting effect of Mn on a Pt/C catalyst for the steam and aqueous phase reforming of glycerol, J. Catal. 349 (2017) 75–83. doi:10.1016/j.jcat.2017.03.002.

[41] L.S. Ribeiro, E.G. Rodrigues, J.J. Delgado, X. Chen, M.F.R. Pereira, J.J.M. Órfão, Pd, Pt, and Pt–Cu catalysts supported on carbon nanotube (CNT) for the selective oxidation of glycerol in alkaline and base-free conditions, Ind. Eng. Chem. Res. 55 (2016) 8548–8556. doi:10.1021/acs.iecr.6b01732.

[42] M.C. Román-Martínez, D. Cazorla-Amorós, A. Linares-Solano, C.S.-M. de Lecea, Tpd and TPR characterization of carbonaceous supports and Pt/C catalysts, Carbon 31 (1993) 895–902. doi:10.1016/0008-6223(93)90190-L.

[43] F. Epron, F. Gauthard, J. Barbier, Influence of oxidizing and reducing treatments on the metal–metal interactions and on the activity for nitrate reduction of a Pt-Cu bimetallic catalyst, Appl. Catal. A Gen. 237 (2002) 253–261. doi:https://doi.org/10.1016/S0926-860X(02)00331-9.

[44] O.S.G.P. Soares, J.J.M. Órfão, J. Ruiz-Martínez, J. Silvestre-Albero, A. Sepúlveda-Escribano, M.F.R. Pereira, Pd–Cu/AC and Pt–Cu/AC catalysts for nitrate reduction with hydrogen: Influence of calcination and reduction temperatures, Chem. Eng. J. 165 (2010) 78–88. doi:https://doi.org/10.1016/j.cej.2010.08.065.

[45] S. Ghosh, R. Das, I.H. Chowdhury, P. Bhanja, M.K. Naskar, Rapid template-free synthesis of an air-stable hierarchical copper nanoassembly and its use as a reusable catalyst for 4-nitrophenol reduction, RSC Adv. 5 (2015) 101519–101524. doi:10.1039/C5RA16644F.

[46] R. Crisafulli, R.M. Antoniassi, A. Oliveira Neto, E. V. Spinacé, Acid-treated PtSn/C and PtSnCu/C electrocatalysts for ethanol electro-oxidation, Int. J. Hydrog. Energy 39 (2014) 5671–5677. doi:10.1016/j.ijhydene.2014.01.111.

[47] R.B. De Lima, V. Paganin, T. Iwasita, W. Vielstich, On the electrocatalysis of ethylene glycol oxidation, Electrochim. Acta. 49 (2003) 85–91. doi:10.1016/j.electacta.2003.05.004.

[48] E. V. Spinacé, A.O. Neto, M. Linardi, Electro-oxidation of ethanol on PtRu/C electrocatalysts prepared from (η-C2H4)(Cl)Pt(μCl)2Ru(Cl)(η 3,η3-C10H16), J. Power Sources. 124 (2003) 426–431. doi:10.1016/S0378-7753(03)00808-5.

[49] E. V. Spinacé, A.O. Neto, M. Linardi, Electro-oxidation of methanol and ethanol using PtRu/C electrocatalysts prepared by spontaneous deposition of platinum on carbon-supported ruthenium nanoparticles, J. Power Sources 129 (2004) 121–126. doi:10.1016/j.jpowsour.2003.11.056.

[50] M. Oezaslan, F. Hasché, P. Strasser, PtCu3, PtCu and Pt3Cu alloy nanoparticle electrocatalysts for oxygen reduction reaction in alkaline and acidic media, J. Electrochem. Soc. 159 (2012) B444. doi:10.1149/2.106204jes.

[51] Y.-C. Tseng, H.-S. Chen, C.-W. Liu, T.-H. Yeh, K.-W. Wang, The effect of alloying on the oxygen reduction reaction activity of carbon-supported PtCu and PtPd nanorods, J. Mater. Chem. A. 2 (2014) 4270–4275. doi:10.1039/C3TA14705C.

[52] T. Kaito, H. Tanaka, H. Mitsumoto, S. Sugawara, K. Shinohara, H. Ariga, H.

Uehara, S. Takakusagi, K. Asakura, Y.-C. Tseng, H.-S. Chen, C.-W. Liu, T.-H. Yeh, K.-W. Wang, In situ X-ray absorption fine structure analysis of PtCo, PtCu, and PtNi alloy electrocatalysts: the correlation of enhanced oxygen reduction reaction activity and structure, J. Phys. Chem. C. 120 (2016) 11519–11527. doi:10.1021/acs.jpcc.6b01736.

[53] M.K. Agusta, H. Kasai, Theoretical study on hydrazine chemisorption on transition metal surfaces, J. Phys. Soc. Japan 81 (2012) 124705. doi:10.1143/JPSJ.81.124705.

[54] J.A. Harrison, Z.A. Khan, The oxidation of hydrazine in alkaline solution at platinum and mercury, J. Electroanal. Chem. Interfacial Electrochem. 26 (1970) 1–11. doi:10.1016/S0022-0728(70)80060-2.

[55] T. Kodera, M. Honda, H. Kita, Electrochemical behaviour of hydrazine on platinum in alkaline solution, Electrochim. Acta. 30 (1985) 669–675. doi:10.1016/0013-4686(85)80110-9.

[56] V. Rosca, M.T.M. Koper, Electrocatalytic oxidation of hydrazine on platinum electrodes in alkaline solutions, Electrochim. Acta. 53 (2008) 5199–5205. doi:10.1016/j.electacta.2008.02.054.

[57] U. Martinez, K. Asazawa, B. Halevi, A. Falase, B. Kiefer, A. Serov, M. Padilla, T. Olson, A. Datye, H. Tanaka, P. Atanassov, Aerosol-derived Ni1−xZnx electrocatalysts for direct hydrazine fuel cells, Phys. Chem. Chem. Phys. 14 (2012) 5512. doi:10.1039/c2cp40546f.

[58] A. Serov, M. Padilla, A.J. Roy, P. Atanassov, T. Sakamoto, K. Asazawa, H. Tanaka, Anode catalysts for direct hydrazine fuel cells: from laboratory test to an electric vehicle, Angew. Chemie. 126 (2014) 10504–10507. doi:10.1002/ange.201404734.

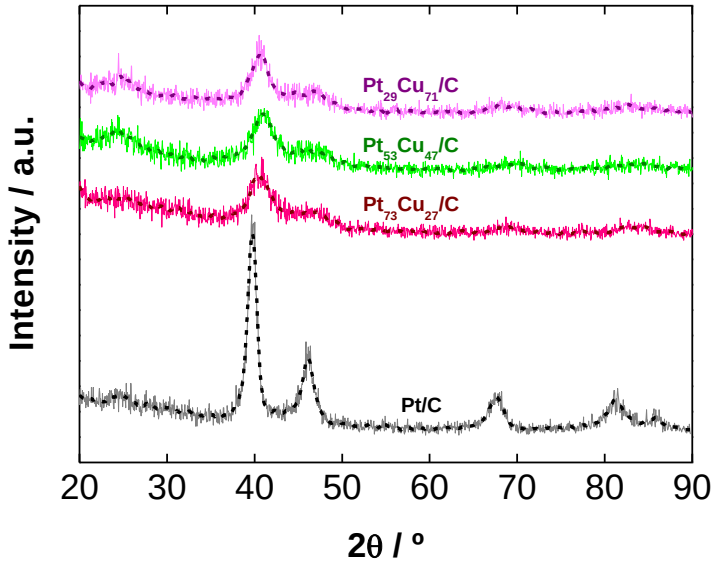

Figure 1. X-ray diffractograms of Pt/C and PtCu/C electrocatalysts

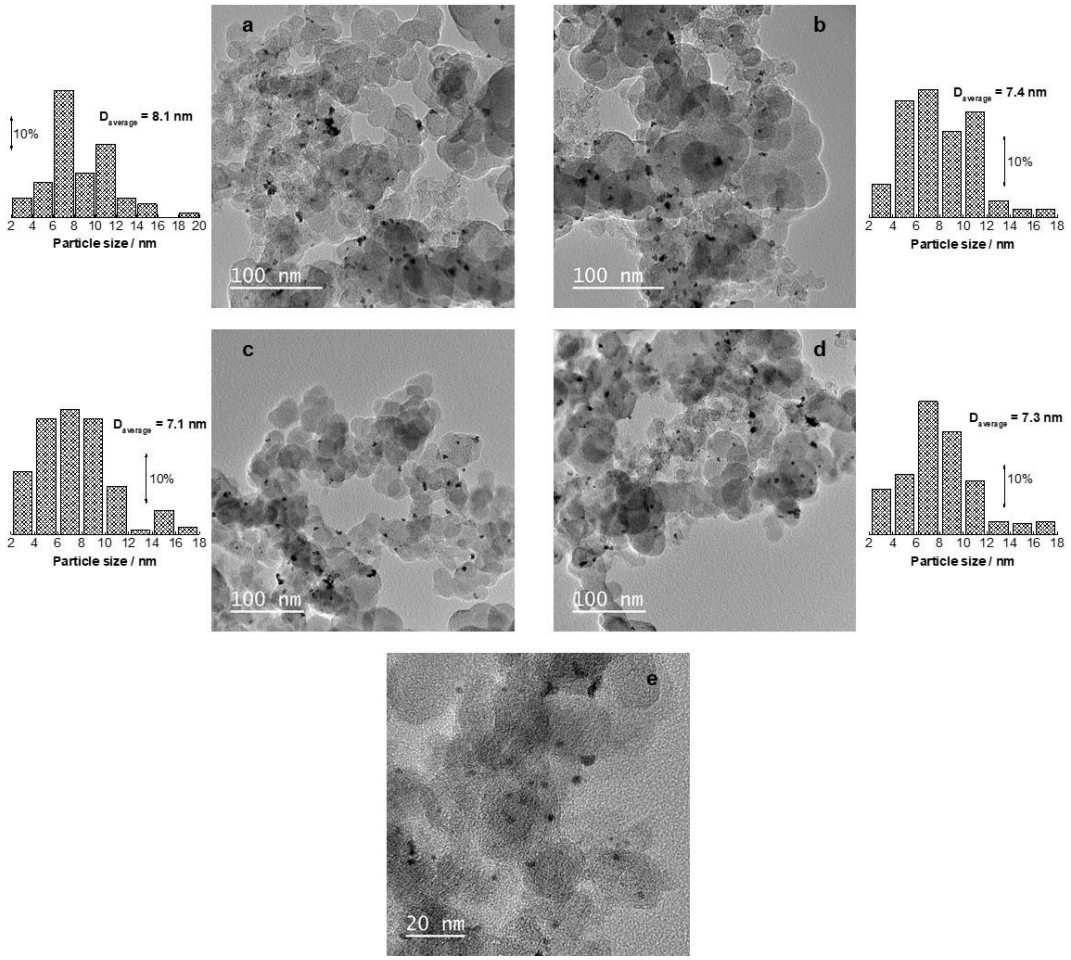

Figure 2. TEM images of the electrocatalysts: a) Pt/C, b) $Pt_{73}Cu_{27}$/C, c) $Pt_{53}Cu_{47}$/C, and d) $Pt_{29}Cu_{71}$/C and e) high-resolution image of the $Pt_{53}Cu_{57}$/C

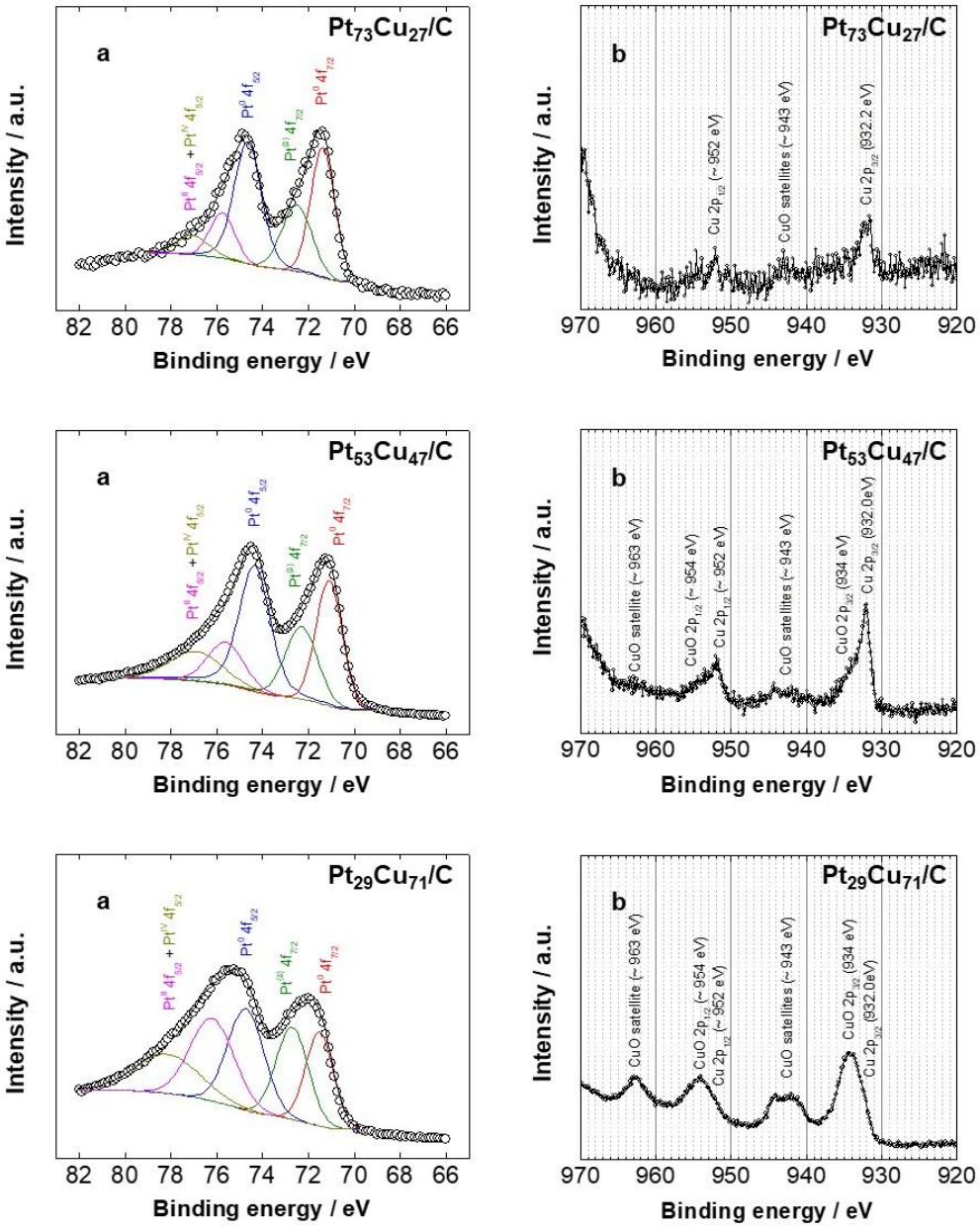

Figure 3. Pt 4*f* (a) and Cu 2*p* (b) XPS spectra of the different electrocatalysts

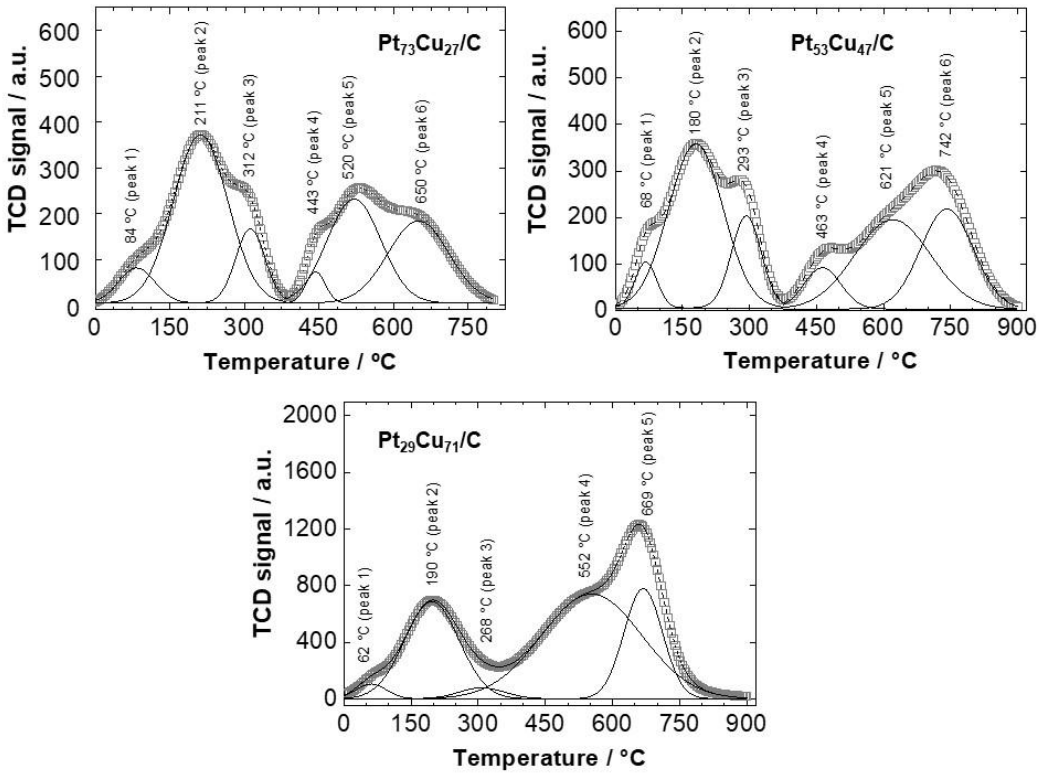

Figure 4. TPR profiles of the different bimetallic electrocatalysts prepared

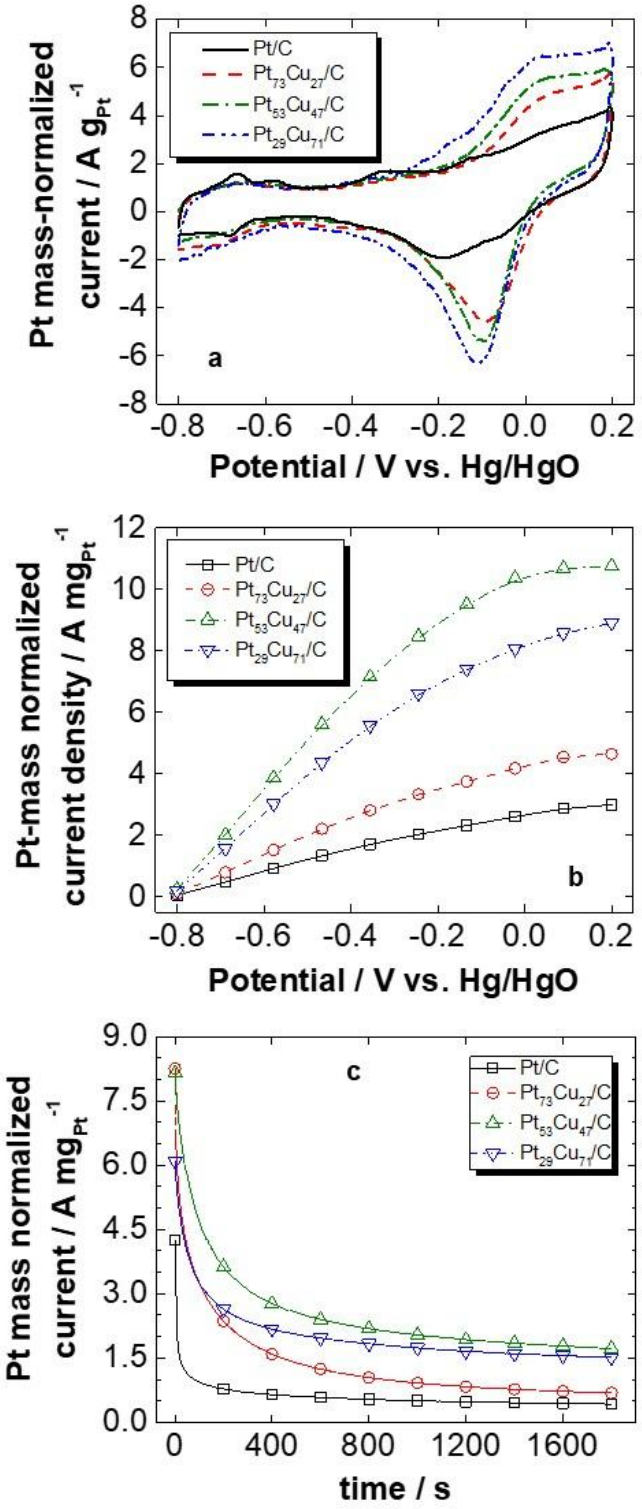

Figure 5. a) Cyclic voltammograms of the different electrocatalysts in 1 mol L^{-1} KOH; b) linear sweep voltammograms in 1 mol L^{-1} KOH and 1 mol L^{-1} hydrazine hydrate; and c) chronoamperograms at 0.024 V vs Hg/HgO in 1 mol L^{-1} KOH and 1 mol L^{-1} hydrazine hydrate

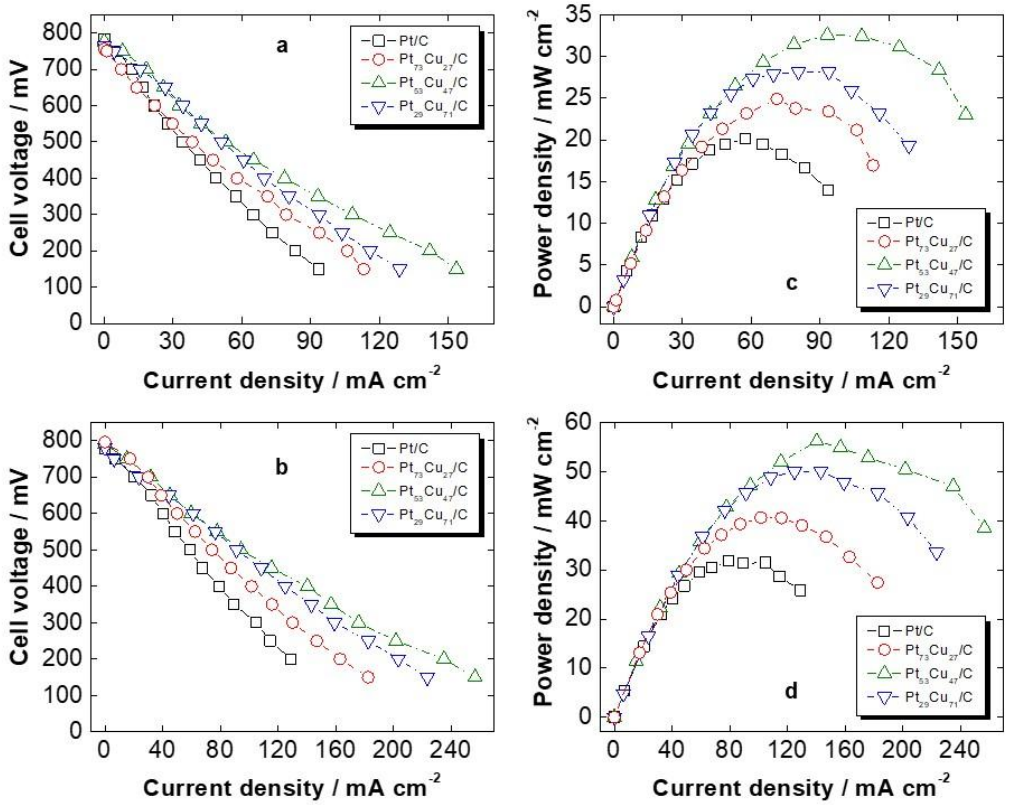

Figure 6. Polarization curves at: a) 60 ºC and b) 80 ºC; power density curves at c) 60 ºC and d) 80 ºC for the different electrocatalysts

Table 1. Pt:Cu atomic ratios for PtCu/C electrocatalysts and weight percentages of metal and carbon loadings for PtCu/C and Pt/C electrocatalysts obtained by EDX.

Electrocatalyst	Carbon loading (wt.%)	Metal loading (wt.%)	**Pt:Cu atomic ratio**	
			Nominal	**EDX**
Pt/C	80	20	–	–
$Pt_{73}Cu_{27}$/C	79	21	75:25	73:27
$Pt_{53}Cu_{47}$/C	82	18	50:50	53:47
$Pt_{29}Cu_{71}$/C	84	16	25:75	29:71

Table 2. Average crystallite sizes and lattice parameters of Pt/C and PtCu/C electrocatalysts obtained by XRD and average particle size obtained from TEM images

Electrocatalyst	Crystallite size (nm)	Lattice parameter (nm)	Cu fraction in the alloy	Fraction of Cu alloyed	Average particle size (nm)
Pt/C	4.6	0.391	–	–	8.1
$Pt_{73}Cu_{27}$/C	2.1	0.387	0.174	0.427	7.4
$Pt_{53}Cu_{47}$/C	2.3	0.382	0.337	0.428	7.1
$Pt_{29}Cu_{71}$/C	2.5	0.386	0.207	0.107	7.3

Table 3. Surface elemental analysis results for PtCu/C electrocatalysts based on XPS data.

Electrocatalyst	Atomic percentage (%)		Platinum oxidation state (%)	
	Pt	Cu	Pt (0)	Pt (δ+)
$Pt_{73}Cu_{27}/C$	77	23	56	44
$Pt_{53}Cu_{47}/C$	60	40	57	43
$Pt_{29}Cu_{71}/C$	41	59	44	56

Table 4. Maximum power density (MPD) values obtained from the power density curves in a single DHFC operating at 60 and 80 °C for Pt/C and PtCu/C electrocatalysts and percentage variation of the MPD of the PtCu/C electrocatalysts in relation to the Pt/C.

Electrocatalyst	DHFC at 60 °C		DHFC at 80 °C	
	MPD (mW cm^{-2})	PI	MPD (mW cm^{-2})	PI
Pt/C	20.1	–	31.5	–
$Pt_{73}Cu_{27}$/C	24.9	23.4	40.7	29.2
$Pt_{53}Cu_{47}$/C	32.6	62.2	56.1	78.1
$Pt_{29}Cu_{71}$/C	28.2	40.3	50.1	59.0

*Graphical Abstract

GRAPHICAL ABSTRACT

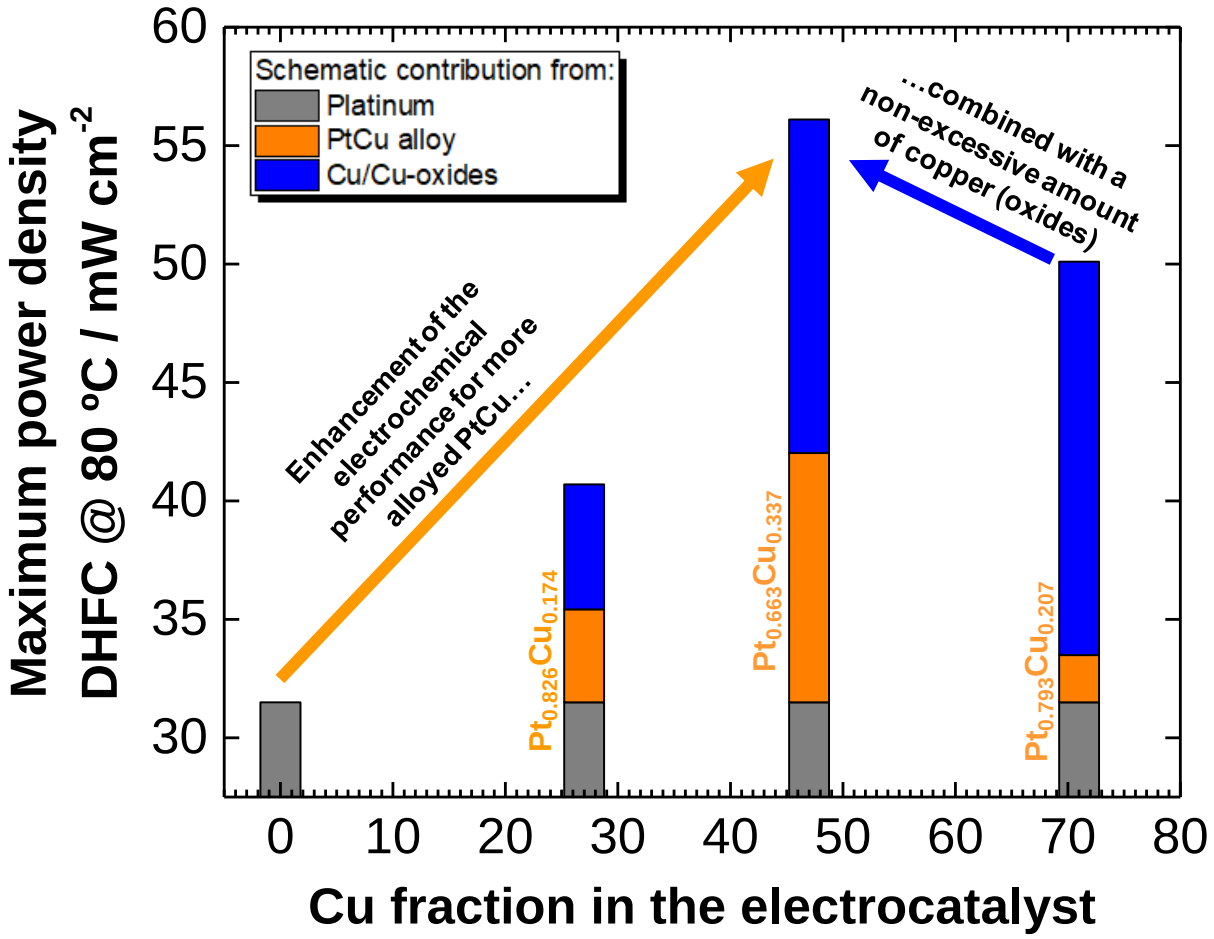

HIGHLIGHTS

- Cu promotes hydrazine electroxidation on Pt in an alkaline environment.
- PtCu alloy exerts a promotional effect on the Pt electronic environment.
- The presence of copper oxides also assists in the hydrazine electroxidation.
- The equiatomic Pt:Cu ratio is the most electrochemically active one.
- A 78.1% increase in the maximum power density compared to Pt/C was achieved.

On the promotional effect of Cu on Pt for hydrazine electrooxidation in alkaline medium

Rudy Crisafulli,[*1] Vanine V. Silva de Barros,[1] Francisca E. Rodrigues de Oliveira,[2] Thairo de Araújo Rocha,[2] Sabrina Zignani,[3] Lorenzo Spadaro,[3] Alessandra Palella,[3] José A. Dias,[4] José J. Linares[*1]

[1] Laboratório de Desenvolvimento de Processos Químicos, Universidade de Brasília, Campus Universitário Darcy Ribeiro, 70910-900 Brasília, Distrito Federal, Brazil

[2] Instituto de Química de São Carlos, Universidade de São Paulo, Av. Trabalhador São-Carlense, 400, 13566-590 São Carlos, SP, Brazil

[3] ITAE – Istituto di Tecnologie Avanzate per l'Energia "Nicola Giordano", Salita Santa Lucia Sopra Contesse, 5, 98126 Messina (ME), Italy

[4] Laboratório de Catálise, Instituto de Química, Universidade de Brasília, Campus Universitário Darcy Ribeiro, Brasília, DF, 70910-900, Brazil.

* Corresponding authors: José J. Linares (Tel.: +556131073828, Fax: +556132734149, Email: joselinares@unb.br); Rudy Crisafulli (Email: rudyunb@gmail.com).

ABSTRACT

Pt/C and PtCu/C electrocatalysts with nominal Pt:Cu atomic ratios of 75:25, 50:50, and 25:75 were prepared using N_2H_4 as reducing agent and carbon black Vulcan XC-72R as support. The obtained materials were physically characterized by X-ray diffraction, Energy-Dispersive X-ray analysis, Transmission Electron Microscopy images, X-ray Photoelectron Spectroscopy (XPS), and Temperature-Programmed Reduction analysis. Cyclic voltammetry, linear sweep voltammetry, and chronoamperometry (TPR) measurements were carried out in a three-electrode glass cell to evaluate the electrochemical activity towards hydrazine electrooxidation in alkaline medium along with single-cell direct hydrazine fuel cell (DHFC) tests. The actual composition of the electrocatalysts evidenced a slightly lower Cu fraction compared to the nominal one. The X-ray diffractograms of the electrocatalysts showed the typical face-centered cubic structure of Pt alloys, with the highest fraction of Cu alloyed to Pt being achieved with the almost equiatomic catalyst. An important fraction of the remaining non-alloyed Cu is in the form of a copper oxide, as evidenced by XPS and TPR measurements. The electrochemical tests evidenced that the coexistence of part of the Cu alloyed with Pt and copper oxide achieved in the PtCu/C electrocatalysts enhances the performance compared to Pt/C. In particular, the optimum formulation is attained by the $Pt_{53}Cu_{47}$/C electrocatalyst, allowing maximization of the electrocatalytic activity towards hydrazine electrooxidation and the single-cell performance at 60 and 80 °C.

Keywords: Direct Hydrazine Fuel Cells; Alkaline Media; Electrocatalysts; PtCu/C.

1. Introduction

Due to operational and infrastructure problems related to the use of hydrogen as fuel in proton exchange membrane fuel cells (PEMFCs) [1-3], liquid fuels have been proposed as an alternative. Their direct oxidation avoids the need to install an onboard reformate system, as proposed for the alcohols [4]. Within the group of liquid fuels, hydrazine appears as a promising candidate. Its synthesis is relatively simple and can be combined with the mass production of ammonia, resulting in a relatively economical fuel.

Hydrazine monohydrate [$N_2H_4 \cdot H_2O$, normal boiling point (NBP) = 121 °C] can be used directly as fuel in PEMFCs: it shows less volatility than the conventional alcohols used in fuel cells (methanol, NBP = 65 ºC; ethanol, NBP = 78 ºC), non-flammability, and a melting temperature of approximately –50 ºC, which makes its use in cold countries feasible [5]. According to the International Agency for Research on Cancer (IARC), hydrazine monohydrate is classified as 2B, like gasoline, so the safety protocols used for handling gasoline may be maintained for hydrazine monohydrate[5]. Furthermore, in Direct Hydrazine Fuel Cells (DHFCs), nitrogen and water are the final byproducts obtained. Furthermore, a high cell voltage with a potential maximum cell voltage of 1.62 V can theoretically be produced by hydrazine electrooxidation (HYEO) and oxygen electroreduction. DHFCs have been operated under acidic and alkaline conditions. In acidic medium, noble metals such as platinum and palladium are generally used [6]. In alkaline medium, other metals such as rhodium, ruthenium, gold, and silver and common metals such as copper also present electrocatalytic activity towards HYEO and have been tested with success in DHFCs [6,7]. Leading investigations have been presented by the Daihatsu Motor Company (Japan) in partnership with Prof. Atanassov's research group and Los Alamos National Laboratory (USA). They present promising electrochemical results accompanied by extensive

physico-chemical characterizations with Pt-free electrocatalysts based on Ni (NiMo/C [8] and $NiO/Nb_2O_5/C$ [9]) in the search for highly active and selective (minimizing the formation of NH_3) material. Furthermore, Sakamoto et al. [10] recently proposed a multi-step reaction DHFC, a promising alternative offering a stable power output over long operating periods. In this approach, both hydrazine and hydrogen (from the chemical decomposition of hydrazine) are used as fuel, allowing a significant reduction of the hydrazine crossover and the formation of radicals from the combination of hydrazine and oxygen in the cathode.

Platinum is considered as a reference material for HYEO. Compton and Aldous [11] showed that in the presence of activated or oxidized Pt, the Pt surface becomes more active, with a significant reduction in the onset potential. On the other hand, as mentioned above, copper, which is more abundant and affordable, is an active material for HYEO, especially in alkaline medium, in both the metallic [12-16] and oxidized forms [16-19]. Moreover, a very recent study presented by de Oliveira et al. [20] demonstrated the importance of the presence of oxidized sites (NiO_x) adjacent to Pt to promote the HYEO through a bifunctional effect. Furthermore, the formation of a PtCu alloy can also lead to changes in the Pt electronic environment that modify the binding energy of the reactants on the catalytic active sites (electronic effect) [21]. In this sense, Karaca et al. [22] have evidenced a significant enhancement when using a PtCu alloy for the hydrolytic dehydrogenation of ammonia and hydrazine borane. Therefore, the preparation of a PtCu electrocatalyst may be of interest for DHFCs if the bifunctional and electronic effects of the formation of the bimetallic alloy and the presence of copper oxides could be combined.

With this background, this paper shows the results of a study in which carbon-supported PtCu bimetallic electrocatalysts with different Pt:Cu atomic proportions have

been prepared by chemical reduction with hydrazine. The catalysts have been physically characterized by X-Ray Diffraction (XRD), Energy-Dispersive X-Ray (EDX) spectroscopy, Transmission Electron Microscopy (TEM), X-ray Photoelectron Spectroscopy (XPS), and Temperature-Programmed Reduction (TPR) to attain a complete description of the prepared materials. The physical and morphological information obtained is subsequently used to assist in interpreting the electrochemical activity for HYEO, which is evaluated by linear sweep voltammetry (LSV) and chronoamperometric studies (CA) in a three-electrode glass cell, and by application as anodes in an alkaline single-cell DHFC.

2. Experimental

Four electrocatalysts with a nominal metal loading of 20 wt.%, Pt, $Pt_{75}Cu_{25}C$, $Pt_{50}Cu_{50}$, and $Pt_{25}Cu_{75}$, deposited on carbon black (Vulcan XC-72R, Cabot Corp.), were prepared by chemical reduction with hydrazine (CRH, $N_2H_4 \cdot H_2O$, Sigma Aldrich). The chemicals $H_2PtCl_6.6H_2O$ (Aldrich) and $CuCl_2.2H_2O$ (Synth) were used as metal sources, while 2-propanol (Synth) and ultra-pure water (Milli-Q, Millipore) were used as solvents. For the preparation of 500 mg of electrocatalysts, the required metal salts were dissolved in 200 mL of a water/2-propanol (90/10 v/v) solution. Subsequently, 400 mg of the carbon support was added to solution and the resulting mixture was sonicated for 30 min. After this time had elapsed, the mixture was placed under vigorous stirring and a reducing solution (50 mL of 2:1 v/v of water/hydrazine) was added at once. The reaction medium was kept under stirring for 30 min at room temperature. Finally, the mixture was filtered and the obtained material was washed with excess water and dried at 70 °C for 2 h.

The Pt:Cu atomic ratios of the bulk of the electrocatalysts were obtained by EDX analysis using a JEOL 2100 scanning electron microscope with a 15-keV electron beam. The XRD analyses were carried out in a Rigaku model D8 Focus diffractometer using Cu K_α radiation (λ = 0.15406 nm). The diffractograms were recorded with 2θ angles in the range of 20 to 90° (0.05º step, 0.5º min^{-1}). The average crystallite (*d*) size was obtained by the application of Scherrer's equation (1), where *K* is a particle-shape-dependent constant (0.9 for spherical particles), λ is the wavelength of the incident radiation (Cu K_α), θ is the angle of the (*hkl*) peak, and $\beta_{(2\theta)}$ is the width in radians of the diffraction peak at half height.

$$d = \frac{K\lambda}{\beta_{(2\theta)} \cos\theta} \quad (1)$$

TEM analysis was performed using a JEOL 2100 microscope operating at 200 kV with point-to-point resolution of 0.19 Å. The particle size distribution was estimated from observations of at least 300 particles in different images. The average particle size, *D*, was calculated according to Equation 2, where n_i represents the number of particles of diameter D_i. The sample holder was composed of a gold grid covered by Lacey carbon (EMS).

$$D = \frac{\sum_i n_i D_i}{\sum_i n_i} \quad (2)$$

XPS measurements were carried out using a Physical Electronics (PHI) 5800-01 spectrometer. A monochromatic Al K_α X-ray source was used at a power of 350 W. Spectra were obtained with pass energies of 58.7 eV for elemental analysis and 11.75 eV for determination of the oxidation states. The pressure in the analysis chamber of the spectrometer was 10^{-9} torr during measurements. The Ag $3d_{5/2}$ peak of an Ag foil was used, after argon sputtering, to check the calibration of the binding energy scale.

Quantitative evaluation of each peak was performed by dividing the integrated peak area by atomic sensitivity factors, which were calculated from the ionization cross-sections, the mean free electron escape depth, and the measured transmission functions of the spectrometer. XPS data were interpreted by using the online library of oxidation states implemented in PHI MultiPak 6.1 software and the PHI *Handbook of X-ray Photoelectron Spectroscopy* [23]. By using this technique, it is possible to obtain information about the outermost layers of the metallic nanoparticles, which are fundamental for the electrocatalytic activity [24].

The TPR profiles were obtained under hydrogen atmosphere in a linear quartz microreactor (i.d. = 4 mm) fed with a 5-vol.% H_2/Ar purified carrier at a rate of 30 sccm. The experiments were carried out in the range of 25 to 900 °C at a heating rate of 10 °C min^{-1}. The weight of sample used was approximately 15 mg. The hydrogen consumption was monitored by a thermal conductivity detector calibrated against the peak area of known amounts of CuO. The resultant TPR data were highly reproducible in terms of the positions of maxima (± 2 °C) and extent of H_2 consumption (± 3 °C).

Electrochemical studies were carried out using the ultra-thin coating technique. Electrochemical measurements were performed in a three-electrode cell using a platinized Pt plate as counter electrode, an Hg/HgO/KOH electrode as reference electrode, and a reticulated vitreous carbon (RVC) working electrode (5 mm in diameter). This electrode was prepared by dispersing 1 mg of the electrocatalysts in 1 mL of 2-propanol. The mixture was sonicated for 10 min; then, with the aid of a chromatographic syringe, 20 μL of the dispersion was transferred onto the surface of the previously polished RVC electrode. The experiments were performed using a μ-Autolab (model Type III) potentiostat/galvanostat coupled to a personal computer and General Purpose Electrochemical System (GPES) software. CV measurements were performed

in a 1.0 mol L^{-1} KOH solution at a scan rate of 10 mV s^{-1}. The study of HYEO was performed at room temperature by LSV and chronoamperometry (for 30 min) at 0.024 V versus Hg/HgO in a solution of 1.0 mol L^{-1} hydrazine in 1.0 mol L^{-1} KOH. The current values obtained were Pt-mass normalized.

DHFC tests were performed on a single cell. Electrodes with an active area of 4 cm^2 were prepared as follows. For the anodes, a catalytic ink containing Pt/C or PtCu/C electrocatalyst (catalyst loading of 0.5 mg Pt cm^{-2} for both monometallic and bimetallic materials) and Nafion® emulsion [5 wt.% emulsion in a mixture of aliphatic alcohols (IonPower), forming 10 wt.% of the total catalyst] was brush-painted onto a carbon cloth (Zoltec PX30) diffusion layer. In a similar way, cathodes were prepared using 20 wt.% Pt/C (BASF fuel cells) using a Pt loading of 1 mg cm^{-2}. The membrane electrode assemblies were prepared by hot pressing the anode and cathode onto a pretreated Tokuyama membrane (24 h in 1 mol L^{-1} KOH solution) at 60 °C for 3 min under a pressure of 40.8 kg_f cm^{-2}. Electrical performances were determined from polarization and power density curves using a single cell at 60 and 80 °C. The fuel was delivered at 2.4 mL min^{-1} through the anode and pure oxygen flow was regulated at 30 sccm for the cathode.

3. Results and discussion

In order to assess the actual Pt:Cu ratios in the electrocatalysts, EDX analyses were carried out. Table 1 lists the corresponding results. In general, the obtained Pt:Cu atomic ratios were similar to the nominal values, with the exception of the electrocatalysts with the highest Cu fraction (Pt:Cu ratio of 25:75), where a higher Pt fraction of 29:71 was obtained. A possible reason for this will be discussed later on, based on the smaller fraction of Cu alloyed to Pt and greater presence of copper oxides,

whose anchorage on the carbon support is partially limited. This could also explain the higher deviation of the metallic content of the catalyst on the carbon support with respect to the nominal 20%; that is, the higher the Cu fraction, the greater the deviation. From now on, the electrocatalysts will be referred to by the actual compositions.

Insert Table 1 near here

Figure 1 shows the X-ray diffractograms of the Pt/C and PtCu/C electrocatalysts. As can be seen, all the diffractograms show a broad peak at about 25°, associated to the (200) facet of the hexagonal graphite structure, and five diffraction peaks at approximate angles of 40, 47, 67, 82, and 87°, associated to the (111), (200), (220), (311), and (222) facets, respectively, of Pt face-centered cubic (FCC) crystalline structure [25]. The (111) reflections of Pt crystalline structure were used to calculate the average crystallite sizes, whose values are listed in Table 2. All the prepared materials present crystallite sizes in the nanometric range (2–4 nm). However, the monometallic Pt/C catalyst shows a higher crystal size than the bimetallic materials. Hence during the formation of the crystallites, Cu (or copper oxide) exerts a protective role, leading to a smaller growth of the embryos formed during the drastic reduction induced by the hydrazine. The diffractograms also evidenced a shift of the peaks relative to Pt (FCC) phase to higher angles compared to those of the Pt/C electrocatalyst, indicating the formation of PtCu alloy [26,27]. Vegard's law can be applied to the PtCu bimetallic system [27-30] according to Equation 3, where a_{PtCu} represents the lattice parameter of the bimetallic material, a_{Pt} the lattice parameter of Pt (0.3912 nm), a_{Cu} the lattice parameter of Cu (0.3601 nm), and x_{Cu} the Cu fraction in the PtCu alloy.

$$a_{PtCu} = x_{Cu} a_{Cu} + (1 - x_{Cu}) a_{Pt} \quad (3)$$

From Equation 2, the Cu fraction in the alloy can be estimated along with the percentage of deposited Cu that is actually alloyed with Pt. For this purpose, Equation 4 must be applied, where $Cu_{alloyed}$ is the amount of Cu in the alloy as a percentage of the total amount of Cu, x is the fraction of copper in the $Pt_{1-x}Cu_x$ alloy, and Cu/Pt is the actual atomic ratio between the two metals.

$$Cu_{alloyed} = \frac{x_{Cu}}{(1 - x_{Cu})\left(Cu/Pt\right)} \quad (4)$$

The corresponding Cu fraction in the alloy and percentage of Cu alloyed are listed in Table 2. As observed, the Cu fraction in the PtCu alloy increases in the sequence from $Pt_{73}Cu_{27}$ to $Pt_{53}Cu_{47}$. The larger fraction of Cu in the catalyst formulation favors a higher Cu insertion in the Pt FCC structure. Oppositely, the $Pt_{29}Cu_{71}$/C shows a decrease in the degree of alloying. A possible explanation for this may be the catalytic role that Pt could play in favoring the Cu(II) reduction and incorporation in the alloy [31]. Indeed, a large fraction of non-alloyed Cu [segregated amorphous metal or copper (I and/or II) oxides] is present in the $Pt_{29}Cu_{71}$/C catalyst. In the other two formulations, the fraction of alloyed Cu remains almost the same, corroborating the important role of the Pt nuclei in forming the PtCu alloy. Higher fractions of alloyed Cu may be achieved by using other reducing agents such as borohydride or by studying the influence of the reduction conditions such as the temperature, reduction time, and/or reducing agent concentration, among others. Moreover, alternative reduction routes, such as the thermal one, may be promising.

Insert Figure 1 near here

Insert Table 2 near here

Figure 2 shows the TEM images of the different electrocatalysts and the corresponding particle size distribution. The average particle sizes are listed in Table 2. As can be observed, although the crystallite domains estimated by XRD are small, they tend to agglomerate, forming larger nanoparticles that are clearly visible in all the materials, leading to average particle sizes between 6 and 8 nm. Furthermore, the size distribution is rather heterogenous (from 2 to 18–20 nm), although small particles can be seen in the high-resolution image obtained for the $Pt_{53}Cu_{47}$/C (2–4 nm, Fig. 2e). The use of a strong reducing agent such as hydrazine may be responsible for these results, which suggests that a capping agent would be necessary to prepare electrocatalysts with a more homogeneous particle size distribution when using the strong reducing agent hydrazine.

Insert Figure 2 near here

The surface composition and oxidation state of platinum and copper on the surface of the $Pt_{73}Cu_{27}$/C, $Pt_{53}Cu_{47}$/C, and $Pt_{29}Cu_{71}$/C electrocatalysts were investigated using XPS. The respective spectra are displayed in Figure 3 and the estimated Pt and Cu percentages in the surface are listed in Table 3. The Pt 4f XPS spectra show the Pt $4f_{7/2}$ and Pt $4f_{5/2}$ peaks for metallic platinum at approximately 71.3 and 74.7 eV, respectively. The Pt spectra also display three peaks at approximately 72.5, 75.5, and 77.4 eV, associated with electronic transitions of 4f electrons of PtO, $Pt(OH)_2$, and PtO_2 species [32-34]. One interesting feature observed in the Pt 4f spectra is the appearance of a more intense signal in the region of highest energy (78–82 eV), where the Cu fraction is higher. A tentative assignment would be the Cu $3p_{1/2}$ signal of the copper oxide [35], in consonance with the greater presence of this species. An estimation of the ratio of metallic to oxidized Pt reveals that the amount of metallic Pt remains almost constant in

the $Pt_{73}Cu_{27}$/C and $Pt_{53}Cu_{47}$/C, whereas Pt oxide species are predominant in the $Pt_{29}Cu_{71}$/C, in which the presence of a larger amount of copper oxides species may induce the formation of surface PtO_x sites. Finally, a very interesting feature observed in the Pt 4f spectra is the downshift of the Pt $4f_{7/2}$ (71.4 eV for $Pt_{73}Cu_{27}$/C, 71.1 eV for $Pt_{53}Cu_{47}$/C, and 71.5 eV for $Pt_{29}Cu_{71}$/C) for the most alloyed electrocatalysts, evidencing an electronic effect of Cu on the sites of the outermost Pt layers. Regarding the Cu 2p spectra, $Pt_{73}Cu_{27}$/C shows tiny peaks at approximately 932 and 952 eV, attributed to metallic copper or cuprous oxide, along with a weak satellite signal ascribed to the presence of small amounts of cupric oxide [27,28,36,37]. These peaks become more evident in the $Pt_{53}Cu_{47}$/C material, at 934 and 954 eV, in addition to the satellites at 943 and 963 eV. The strongest evidences of the presence of CuO are observable in the $Pt_{29}Cu_{71}$/C. Hence, the higher the fraction of Cu, the larger the tendency to form copper oxide species, whose presence may induce the larger fraction of surface Pt oxides.

Insert Figure 3 near here

Insert Table 3 near here

Table 3 also lists the Pt:Cu surface composition. As can be seen, a comparison between the actual ratio of metals and the surface one reveals a certain enrichment of Pt. This result may be explained in terms of a possible galvanic displacement of the nanometallic copper nanoparticles formed during the reduction process by the Pt precursor [38]. Metallic copper then transforms into Cu(II) species. The higher the Cu content in the catalyst formulation, the more severe this phenomenon would be, which could explain the more prominent CuO peaks observed in the XPS spectra. Furthermore, soluble Cu^{2+} could be formed, which would support the reduction of the

metallic content observed in the EDX results at a higher Cu fraction in the catalyst formulation and greater Pt enrichment in the catalyst surface.

Figure 4 shows the TPR signals of the $Pt_{73}Cu_{27}$/C, $Pt_{53}Cu_{47}$/C, and $Pt_{29}Cu_{71}$/C electrocatalysts. As can be observed, all the materials present an initial reduction peak (peak 1) at low temperature (60–80 °C). This temperature relatively low compared to others reported in the literature for Pt/C catalysts (in the range of 100–200 °C [39-42]). This peak is attributed to the reduction of surface platinum oxides. Subsequently, a larger peak (peak 2) appears in the range of 180 to 210 °C for all the materials. This peak can be ascribed to the mixed reduction of both metals in the PtCu alloy [43,44]. Furthermore, this peak can contain a contribution from copper oxides, which are reduced at lower temperature (approx. 200 °C) in the presence of Pt [41]. Furthermore, the most alloyed electrocatalyst possesses the lowest temperature for the maximum in the signal compared to the other catalysts, corroborating that the Pt can exert a spillover effect on copper oxides. The third and fourth peaks in the first low-temperature region of the TPR profiles appear in the ranges of 290–310 °C and 440–460 °C in the $Pt_{73}Cu_{27}$/C and $Pt_{53}Cu_{47}$/C catalysts. According to the literature [43] (and in agreement with the XPS spectra), those peaks may be assigned to the reduction of Cu_2O and CuO species that are not interacting with Pt. It is interesting to note that in the $Pt_{53}Cu_{47}$/C, the area of the peaks is larger (a larger Cu fraction), although their proportions are similar. Thus it can be speculated that, in percentage terms, the copper speciation is similar in both materials. Finally, two large peaks can be observed above 500 °C (peaks 5 and 6 of $Pt_{73}Cu_{27}$/C and $Pt_{53}Cu_{47}$/C). These can be ascribed to gasification of the carbon support [39], even though large Cu_2O/CuO particle sizes may also contribute to the lowest temperature peak [45]. In the case of the $Pt_{29}Cu_{71}$/C, a very weak peak can be identified at 268 °C (peak 3) and is tentatively assigned to a small amount of cuprous oxide. The

fourth peak, centered at 552 °C, may contain a simultaneous contribution from the predominant cupric oxide and support gasification. The final peak (peak 5, > 650 °C) is assigned to gasification of the carbon support. A very interesting feature of the TPR profiles is the increase observed in the TCD signal as the Cu fraction in the electrocatalysts increases, with special significance in the case of the $Pt_{29}Cu_{71}$/C, confirming the larger amount of oxidized species deposited on the carbon support.

Insert Figure 4 near here

Figure 5a displays the corresponding cyclic voltammograms in alkaline medium (1 mol L^{-1} KOH) of Pt/C and the PtCu/C electrocatalysts. As can be seen, the profiles of the PtCu/C electrocatalysts do not show the characteristic anodic stripping peaks associated with the hydrogen adsorption/desorption on Pt surface atoms (–0.8 to –0.5 V vs. Hg/HgO) typical of Pt/C. This is a consequence of inhibition of the hydrogen adsorption/oxidation processes over Pt and can be attributed to the incorporation of copper within the structure of platinum on the PtCu/C electrocatalyst surfaces [46]. Also, the PtCu/C electrocatalysts show an increase in the currents in the double layer (–0.55 and 0.3 V vs. Hg/HgO) with increasing copper content, which is ascribed to the growing presence of copper oxides [47-49]. Finally, larger currents are observed in the regions of Pt-oxide formation/reduction, whose intensification is due to important contributions from copper redox pairs [50]. This feature becomes more evident at the higher Cu fraction as a result of the more Cu-enriched surface.

The electrochemical activity towards HYEO is assessed by LSV. Figure 5b displays the corresponding profiles. As can be observed, the HYEO activity improves notably when Cu is added to the catalyst formulation. In the literature [51,52], the formation of a PtCu alloy leads to a reduction of the unfilled Pt 5d states, lowering the adsorption strengths (of the eventual adsorbates formed) compared to Pt [53] and

diminishing the tendency to form platinum oxide at high potential. Two pieces of evidence can support this statement: the lower binding energy observed for the $Pt_{57}Cu_{47}/C$ in the Pt $4f_{7/2}$ region of the XPS spectra and the lower reduction temperature of Pt oxide species in the bimetallic materials. These features are indeed important. According to the literature [20], non-oxidized Pt sites are required for complete HYEO, where dissociative adsorption [20,54-56] takes place in order to produce adsorbed $N_2H_{x,ads}$ and H_{ads} species that are subsequently oxidized by adsorbed OH_{ads} and/or OH^-. The lower tendency to form Pt oxides in the alloyed PtCu along with the expected weaker adsorption strength can intrinsically accelerate the HYEO dissociative adsorption steps on Pt (electronic effect). On the other hand, the presence of oxidized copper species may contribute, through the bifunctional mechanism, by providing OH_{ads} species after OH^- discharge. Finally, copper/copper oxide species are active for HYEO, as stated in the Introduction. The combination of all these factors explains the enhanced electrochemical performance of the PtCu electrocatalysts. Regarding the composition, the most adequate (balanced) material is the almost equiatomic $Pt_{53}Cu_{47}/C$, in which almost half of the copper forms, with Pt, the most alloyed electrocatalyst in combination with an optimum amount of surface copper/copper oxides. In the $Pt_{73}Cu_{27}/C$, the lower degree of alloying attained and the reduced presence of copper diminish the electrochemical performance. The $Pt_{29}Cu_{71}/C$ also presents a lower degree of alloying and a high fraction of Cu species on the catalytic surface, limiting its performance. The presence of the active copper phase may reduce the size of the observed performance drop compared to $Pt_{73}Cu_{27}/C$. The chronoamperometric curves shown in Figure 5c confirm these results.

Insert Figure 5 near here

Insert Table 3 near here

Figures 6a and 6b show the polarization curves, while Figs. 6c and 6d display the power density curves in a single DHFC operating at 60 and 80 °C, using $Pt_{73}Cu_{27}$/C, $Pt_{53}Cu_{47}$/C, $Pt_{29}Cu_{71}$/C, and Pt/C electrocatalysts as anodes. As can be observed, the polarization curves confirm that, regardless of the temperature, the $Pt_{53}Cu_{47}$/C is the most active material with the highest current densities, as seen in the three-electrode glass cell. These results are also corroborated by the power densities at 60 and 80 ºC. Table 4 lists the maximum power densities (MPDs) and performance improvements (PIs) with respect to the Pt/C electrocatalyst, and it can be seen that the highest values were found for the $Pt_{53}Cu_{47}$/C. In this material, it is possible to achieve the maximum fraction of PtCu alloy with the optimum fraction of copper oxides present in the surface. The lower degree of alloying of the other two PtCu electrocatalysts and, particularly, the reduced amount of copper/copper oxides in the $Pt_{73}Cu_{27}$/C explain the observed sequence $Pt_{53}Cu_{47}$/C > $Pt_{29}Cu_{71}$/C > $Pt_{73}Cu_{27}$/C > Pt/C. Finally, it is interesting to observe that the PI becomes stronger as the temperature increases. This could be explained by the activation of the Cu phase, which reinforces the auxiliary effects discussed extensively above. Thus, the potential to reduce noble metal loading in this application is consistent with other studies such as [57,58], which also show potential for high-performance DHFC technology utilizing either low- or non-noble metal electrocatalysts.

Insert Figure 6 near here

Insert Table 4 near here

4. Conclusions

This study demonstrates the promotional effect of copper on the electrocatalytic activity for HYEO of platinum. The formation of a PtCu alloy seems to alter the electronic

environment favorably and is balanced by the presence of Cu oxide species that can donate OH_{ads} for completion of the HYEO, leading to a very active material for application in DHFCs. Despite some particle agglomeration due to the use of hydrazine as a strong reducing agent, the different highly electroactive Pt_xCu_{100-x}/C electrocatalysts outperform the reference Pt/C (also prepared by CRH). Regarding the Pt:Cu ratio, the highest performance is achieved with the almost equiatomic $Pt_{53}Cu_{47}/C$, whose electrocatalytic surface attains an optimum equilibrium between the largest fraction of Cu alloyed with Pt and the presence of active copper oxides. A lower Cu content in the catalyst formulation reduces the degree of alloying and especially the fraction of copper oxides. A higher Cu content also reduces the degree of alloying in these materials prepared by CRH, reducing the electronic effect despite the larger fraction of copper oxides. In this scenario, the electrochemical performances studied in a more fundamental glass cell and in an actual single DHFC lead to the following sequence of electroactive materials for HYEO: $Pt_{53}Cu_{47}/C > Pt_{29}Cu_{71}/C > Pt_{73}Cu_{27}/C >$ Pt/C.

Acknowledgments

The authors thank Coordenação de Aperfeiçoamento de Pessoal de Nível Superior (CAPES) for a scholarship awarded to Rudy Crisafulli. In addition, we acknowledge the research scholarship provided by CNPq and financial support provided by UnB/DPI/IQ, MCTI/CNPq, CAPES, FAP-DF, and FINEP/CTPetro.

References

[1] R. Moliner, M.J. Lazaro, I. Suelves, Analysis of the strategies for bridging the gap towards the hydrogen economy, Int. J. Hydrog. Energy 41 (2016) 19500–

19508. doi:10.1016/j.ijhydene.2016.06.202.

[2] M. Ball, M. Weeda, The hydrogen economy—Vision or reality? Int. J. Hydrog. Energy 40 (2015) 7903–7919. doi:10.1016/j.ijhydene.2015.04.032.

[3] R.M. Antoniassi, J.C.M. Silva, A. Oliveira Neto, E. V Spinacé, Synthesis of Pt+SnO2/C electrocatalysts containing Pt nanoparticles with preferential (100) orientation for direct ethanol fuel cell, Appl. Catal. B Environ. 218 (2017) 91–100. doi:10.1016/j.apcatb.2017.06.031.

[4] L. An, T.S. Zhao, S.Y. Shen, Q.X. Wu, R. Chen, Performance of a direct ethylene glycol fuel cell with an anion-exchange membrane, Int. J. Hydrog. Energy 35 (2010) 4329–4335. doi:10.1016/j.ijhydene.2010.02.009.

[5] T. Sakamoto, K. Asazawa, U. Martinez, B. Halevi, T. Suzuki, S. Arai, D. Matsumura, Y. Nishihata, P. Atanassov, H. Tanaka, Electrooxidation of hydrazine hydrate using Ni-La catalyst for anion exchange membrane fuel cells, J. Power Sources 234 (2013) 252–259. doi:10.1016/j.jpowsour.2013.01.181.

[6] A. Serov, C. Kwak, Direct hydrazine fuel cells: A review, Appl. Catal. B Environ. 98 (2010) 1–9. doi:10.1016/j.apcatb.2010.05.005.

[7] D.A. Finkelstein, R. Imbeault, S. Garbarino, L. Roué, D. Guay, Trends in catalysis and catalyst cost effectiveness for N2H4 fuel cells and sensors: a rotating disk electrode (RDE) study, J. Phys. Chem. C. 120 (2016) 4717–4738. doi:10.1021/acs.jpcc.5b10156.

[8] T. Asset, A. Roy, T. Sakamoto, M. Padilla, I. Matanovic, K. Artyushkova, A. Serov, F. Maillard, M. Chatenet, K. Asazawa, H. Tanaka, P. Atanassov, Highly active and selective nickel molybdenum catalysts for direct hydrazine fuel cell, Electrochim. Acta. 215 (2016) 420–426. doi:10.1016/j.electacta.2016.08.106.

[9] T. Sakamoto, T. Masuda, K. Yoshimoto, H. Kishi, S. Yamaguchi, D. Matsumura, K. Tamura, A. Hori, Y. Horiuchi, A. Serov, K. Artyushkova, P. Atanassov, H. Tanaka, NiO/Nb2O5/C hydrazine electrooxidation catalysts for anion exchange membrane fuel cells, J. Electrochem. Soc. 164 (2017) F229–F234. doi:10.1149/2.0281704jes.

[10] T. Sakamoto, A. Serov, T. Masuda, M. Kamakura, K. Yoshimoto, T. Omata, H. Kishi, S. Yamaguchi, A. Hori, Y. Horiuchi, T. Terada, K. Artyushkova, P. Atanassov, H. Tanaka, Highly durable direct hydrazine hydrate anion exchange membrane fuel cell, J. Power Sources 375 (2018) 291–299. doi:10.1016/j.jpowsour.2017.05.052.

[11] L. Aldous, R.G. Compton, The mechanism of hydrazine electro-oxidation revealed by platinum microelectrodes: role of residual oxides, Phys. Chem. Chem. Phys. 13 (2011) 5279–5287. doi:10.1039/C0CP02261F.

[12] F. Jia, J. Zhao, X. Yu, Nanoporous Cu film/Cu plate with superior catalytic performance toward electro-oxidation of hydrazine, J. Power Sources 222 (2013) 135–139. doi:10.1016/j.jpowsour.2012.08.076.

[13] E. Granot, B. Filanovsky, I. Presman, I. Kuras, F. Patolsky, Hydrazine / air direct-liquid fuel cell based on nanostructured copper anodes, J. Power Sources 204 (2012) 116–121. doi:10.1016/j.jpowsour.2011.12.008.

[14] S. Lal, M. Deepa, V.M. Janardhanan, K.C. Sahu, Paper based hydrazine monohydrate fuel cells with Cu and C composite catalysts, Electrochim. Acta.

232 (2017) 262–270. doi:10.1016/j.electacta.2017.02.118.

[15] H. Gao, Y. Wang, F. Xiao, C.B. Ching, H. Duan, Growth of copper nanocubes on graphene paper as free-standing electrodes for direct hydrazine fuel cells, J. Phys. Chem. C. 116 (2012) 7719–7725. doi:10.1021/jp3021276.

[16] G. Karim-Nezhad, R. Jafarloo, P.S. Dorraji, Copper (hydr)oxide modified copper electrode for electrocatalytic oxidation of hydrazine in alkaline media, Electrochim. Acta. 54 (2009) 5721–5726. doi:10.1016/j.electacta.2009.05.019.

[17] Y. Ma, H. Li, R. Wang, H. Wang, W. Lv, S. Ji, Ultrathin willow-like CuO nanoflakes as an efficient catalyst for electro-oxidation of hydrazine, J. Power Sources 289 (2015) 22–25. doi:10.1016/j.jpowsour.2015.04.151.

[18] S.R. Hosseini, M. Kamali-Rousta, Preparation of electro-spun CuO nanoparticle and its application for hydrazine hydrate electro-oxidation, Electrochim. Acta. 189 (2016) 45–53. doi:10.1016/j.electacta.2015.12.070.

[19] R.A. Soomro, Q. Baloach, A. Tahira, Z.H. Ibupoto, G.Q. Khaskheli, Sirajuddin, V.K. Deewani, K.R. Hallam, K. Rajar, M. Willander, Rice-like CuO nanostructures for sensitive electrochemical sensing of hydrazine, Microsyst. Technol. 23 (2017) 731–738. doi:10.1007/s00542-015-2726-x.

[20] D.C. de Oliveira, W.O. Silva, M. Chatenet, F.H.B.B. Lima, NiOx-Pt/C nanocomposites: Highly active electrocatalysts for the electrochemical oxidation of hydrazine, Appl. Catal. B Environ. 201 (2017) 22–28. doi:10.1016/j.apcatb.2016.08.007.

[21] S. Mukerjee, S. Srinivasan, M.P. Soriaga, J. McBreen, Role of structural and electronic properties of Pt and Pt alloys on electrocatalysis of oxygen reduction: an in situ XANES and EXAFS investigation, J. Electrochem. Soc. 142 (1995) 1409–1422. doi:10.1149/1.2048590.

[22] T. Karaca, M. Sevim, Ö. Metin, Facile synthesis of monodisperse copper–platinum alloy nanoparticles and their superb catalysis in the hydrolytic dehydrogenation of ammonia borane and hydrazine borane, ChemCatChem. 9 (2017) 4185–4190. doi:10.1002/cctc.201701023.

[23] J.F. Moulder, W.F. Stickle, P.E. Sobol, K.D. Bomben, Handbook of X-ray Photoelectron Spectroscopy, 1st ed., Perkin-Elmer Corporation, 1992.

[24] S. Liao, B. Li, Y. Li, Physical characterization of electrocatalysts, in: J. Zhang (Ed.), PEM Fuel Cell Electrocatalysts and Catalyst Layers: Fundamentals and Applications, Springer London, London, 2008, pp. 487–546. doi:10.1007/978-1-84800-936-3_10.

[25] J.W. Edwards, R. Speiser, H.L. Johnston, High temperature structure and thermal expansion of some metals as determined by X-Ray diffraction data. I. Platinum, tantalum, niobium, and molybdenum, J. Appl. Phys. 22 (1951) 424–428. doi:10.1063/1.1699977.

[26] W.J. Zhou, S.Q. Song, W.Z. Li, G.Q. Sun, Q. Xin, S. Kontou, K. Poulianitis, P. Tsiakaras, Pt-based anode catalysts for direct ethanol fuel cells, Solid State Ion. 175 (2004) 797–803. doi:10.1016/j.ssi.2004.09.055.

[27] E.A. Carbonio, F. Colmati, E.G. Ciapina, M.E. Pereira, E.R. Gonzalez, Pt-Cu/C and Pd Modified Pt-Cu/C electrocatalysts for the oxygen reduction reaction in

direct methanol fuel cells, J. Braz. Chem. Soc. 21 (2010) 590–602. doi: 10.1590/S0103-50532010000400003.

[28] E. Taylor, Synthesis of platinum and platinum-copper branched nanoparticles for electrooxidation of methanol, University of Arkansas, 2013. http://scholarworks.uark.edu/etd (accessed January 17, 2018).

[29] M. Millán, H. Zamora, M.A. Rodrigo, J. Lobato, Enhancement of electrode stability using platinum–cobalt nanocrystals on a novel composite SiCTiC support, ACS Appl. Mater. Interfaces 9 (2017) 5927–5936. doi:10.1021/acsami.6b13071.

[30] J. Lobato, P. Cañizares, M.A. Rodrigo, J.J. Linares, Study of different bimetallic anodic catalysts supported on carbon for a high temperature polybenzimidazole-based direct ethanol fuel cell, Appl. Catal. B Environ. 91 (2009) 269–274. doi:10.1016/j.apcatb.2009.05.035.

[31] M. Gong, Z. Yao, F. Lai, Y. Chen, Y. Tang, Platinum–copper alloy nanocrystals supported on reduced graphene oxide: One-pot synthesis and electrocatalytic applications, Carbon 91 (2015) 338–345. doi:10.1016/j.carbon.2015.05.006.

[32] K. Zhang, Q. Yue, G. Chen, Y. Zhai, L. Wang, H. Wang, J. Zhao, J. Liu, J. Jia, H. Li, Effects of acid treatment of Pt−Ni alloy nanoparticles@graphene on the kinetics of the oxygen reduction reaction in acidic and alkaline solutions, J. Phys. Chem. C. 115 (2011) 379–389. doi:10.1021/jp108305v.

[33] F. Papa, C. Negrila, G. Dobrescu, A. Miyazaki, I. Balint, Preparation, characterization and catalytic behavior of Pt-Cu nanoparticles in methane combustion, J. Nat. Gas Chem. 20 (2011) 537–542. doi:10.1016/S1003-9953(10)60221-6.

[34] S. Fu, C. Zhu, Q. Shi, D. Du, Y. Lin, Enhanced electrocatalytic activities of three dimensional PtCu@Pt bimetallic alloy nanofoams for oxygen reduction reaction, Catal. Sci. Technol. 6 (2016) 5052–5059. doi:10.1039/C5CY02288F.

[35] X. Du, S. Luo, H. Du, M. Tang, X. Huang, P.K. Shen, Monodisperse and self-assembled Pt-Cu nanoparticles as an efficient electrocatalyst for the methanol oxidation reaction, J. Mater. Chem. A. 4 (2016) 1579–1585. doi:10.1039/C5TA09261B.

[36] J.M. Machefert, A. D'Huysser, M. Lenglet, J. Lopitaux, D. Delahaye, Initial stage of copper thermal oxidation studied by UV-vis-NIR reflectance spectroscopy, XPS and X-ray diffraction, Mater. Res. Bull. 23 (1988) 1379–1388. doi:10.1016/0025-5408(88)90262-0.

[37] T.H. Fleisch, G.J. Mains, Reduction of copper oxides by UV radiation and atomic hydrogen studied by XPS, Appl. Surf. Sci. 10 (1982) 51–62. doi:10.1016/0378-5963(82)90134-9.

[38] A. Sarkar, A. Manthiram, Synthesis of Pt@Cu core−shell nanoparticles by galvanic displacement of Cu by Pt4+ ions and their application as electrocatalysts for oxygen reduction reaction in fuel cells, J. Phys. Chem. C. 114 (2010) 4725–4732. doi:10.1021/jp908933r.

[39] A. Ciftci, D.A.J.M. Ligthart, E.J.M. Hensen, Aqueous phase reforming of glycerol over Re-promoted Pt and Rh catalysts, Green Chem. 16 (2014) 853–863. doi:10.1039/C3GC42046A.

[40] F. Bossola, X.I. Pereira-Hernández, C. Evangelisti, Y. Wang, V. Dal Santo, Investigation of the promoting effect of Mn on a Pt/C catalyst for the steam and aqueous phase reforming of glycerol, J. Catal. 349 (2017) 75–83. doi:10.1016/j.jcat.2017.03.002.

[41] L.S. Ribeiro, E.G. Rodrigues, J.J. Delgado, X. Chen, M.F.R. Pereira, J.J.M. Órfão, Pd, Pt, and Pt–Cu catalysts supported on carbon nanotube (CNT) for the selective oxidation of glycerol in alkaline and base-free conditions, Ind. Eng. Chem. Res. 55 (2016) 8548–8556. doi:10.1021/acs.iecr.6b01732.

[42] M.C. Román-Martínez, D. Cazorla-Amorós, A. Linares-Solano, C.S.-M. de Lecea, Tpd and TPR characterization of carbonaceous supports and Pt/C catalysts, Carbon 31 (1993) 895–902. doi:10.1016/0008-6223(93)90190-L.

[43] F. Epron, F. Gauthard, J. Barbier, Influence of oxidizing and reducing treatments on the metal–metal interactions and on the activity for nitrate reduction of a Pt-Cu bimetallic catalyst, Appl. Catal. A Gen. 237 (2002) 253–261. doi:https://doi.org/10.1016/S0926-860X(02)00331-9.

[44] O.S.G.P. Soares, J.J.M. Órfão, J. Ruiz-Martínez, J. Silvestre-Albero, A. Sepúlveda-Escribano, M.F.R. Pereira, Pd–Cu/AC and Pt–Cu/AC catalysts for nitrate reduction with hydrogen: Influence of calcination and reduction temperatures, Chem. Eng. J. 165 (2010) 78–88. doi:https://doi.org/10.1016/j.cej.2010.08.065.

[45] S. Ghosh, R. Das, I.H. Chowdhury, P. Bhanja, M.K. Naskar, Rapid template-free synthesis of an air-stable hierarchical copper nanoassembly and its use as a reusable catalyst for 4-nitrophenol reduction, RSC Adv. 5 (2015) 101519–101524. doi:10.1039/C5RA16644F.

[46] R. Crisafulli, R.M. Antoniassi, A. Oliveira Neto, E. V. Spinacé, Acid-treated PtSn/C and PtSnCu/C electrocatalysts for ethanol electro-oxidation, Int. J. Hydrog. Energy 39 (2014) 5671–5677. doi:10.1016/j.ijhydene.2014.01.111.

[47] R.B. De Lima, V. Paganin, T. Iwasita, W. Vielstich, On the electrocatalysis of ethylene glycol oxidation, Electrochim. Acta. 49 (2003) 85–91. doi:10.1016/j.electacta.2003.05.004.

[48] E. V. Spinacé, A.O. Neto, M. Linardi, Electro-oxidation of ethanol on PtRu/C electrocatalysts prepared from (η-C2H4)(Cl)Pt(μCl)2Ru(Cl)(η 3,η3-C10H16), J. Power Sources. 124 (2003) 426–431. doi:10.1016/S0378-7753(03)00808-5.

[49] E. V. Spinacé, A.O. Neto, M. Linardi, Electro-oxidation of methanol and ethanol using PtRu/C electrocatalysts prepared by spontaneous deposition of platinum on carbon-supported ruthenium nanoparticles, J. Power Sources 129 (2004) 121–126. doi:10.1016/j.jpowsour.2003.11.056.

[50] M. Oezaslan, F. Hasché, P. Strasser, PtCu3, PtCu and Pt3Cu alloy nanoparticle electrocatalysts for oxygen reduction reaction in alkaline and acidic media, J. Electrochem. Soc. 159 (2012) B444. doi:10.1149/2.106204jes.

[51] Y.-C. Tseng, H.-S. Chen, C.-W. Liu, T.-H. Yeh, K.-W. Wang, The effect of alloying on the oxygen reduction reaction activity of carbon-supported PtCu and PtPd nanorods, J. Mater. Chem. A. 2 (2014) 4270–4275. doi:10.1039/C3TA14705C.

[52] T. Kaito, H. Tanaka, H. Mitsumoto, S. Sugawara, K. Shinohara, H. Ariga, H.

Uehara, S. Takakusagi, K. Asakura, Y.-C. Tseng, H.-S. Chen, C.-W. Liu, T.-H. Yeh, K.-W. Wang, In situ X-ray absorption fine structure analysis of PtCo, PtCu, and PtNi alloy electrocatalysts: the correlation of enhanced oxygen reduction reaction activity and structure, J. Phys. Chem. C. 120 (2016) 11519–11527. doi:10.1021/acs.jpcc.6b01736.

[53] M.K. Agusta, H. Kasai, Theoretical study on hydrazine chemisorption on transition metal surfaces, J. Phys. Soc. Japan 81 (2012) 124705. doi:10.1143/JPSJ.81.124705.

[54] J.A. Harrison, Z.A. Khan, The oxidation of hydrazine in alkaline solution at platinum and mercury, J. Electroanal. Chem. Interfacial Electrochem. 26 (1970) 1–11. doi:10.1016/S0022-0728(70)80060-2.

[55] T. Kodera, M. Honda, H. Kita, Electrochemical behaviour of hydrazine on platinum in alkaline solution, Electrochim. Acta. 30 (1985) 669–675. doi:10.1016/0013-4686(85)80110-9.

[56] V. Rosca, M.T.M. Koper, Electrocatalytic oxidation of hydrazine on platinum electrodes in alkaline solutions, Electrochim. Acta. 53 (2008) 5199–5205. doi:10.1016/j.electacta.2008.02.054.

[57] U. Martinez, K. Asazawa, B. Halevi, A. Falase, B. Kiefer, A. Serov, M. Padilla, T. Olson, A. Datye, H. Tanaka, P. Atanassov, Aerosol-derived Ni1−xZnx electrocatalysts for direct hydrazine fuel cells, Phys. Chem. Chem. Phys. 14 (2012) 5512. doi:10.1039/c2cp40546f.

[58] A. Serov, M. Padilla, A.J. Roy, P. Atanassov, T. Sakamoto, K. Asazawa, H. Tanaka, Anode catalysts for direct hydrazine fuel cells: from laboratory test to an electric vehicle, Angew. Chemie. 126 (2014) 10504–10507. doi:10.1002/ange.201404734.

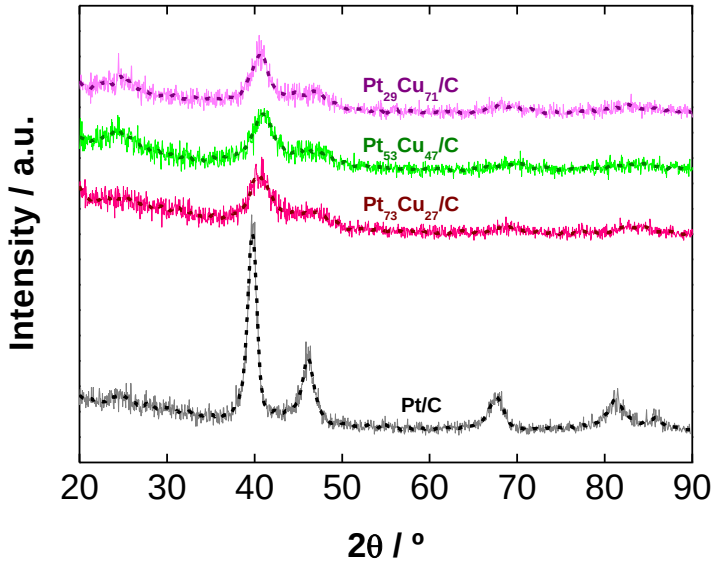

Figure 1. X-ray diffractograms of Pt/C and PtCu/C electrocatalysts

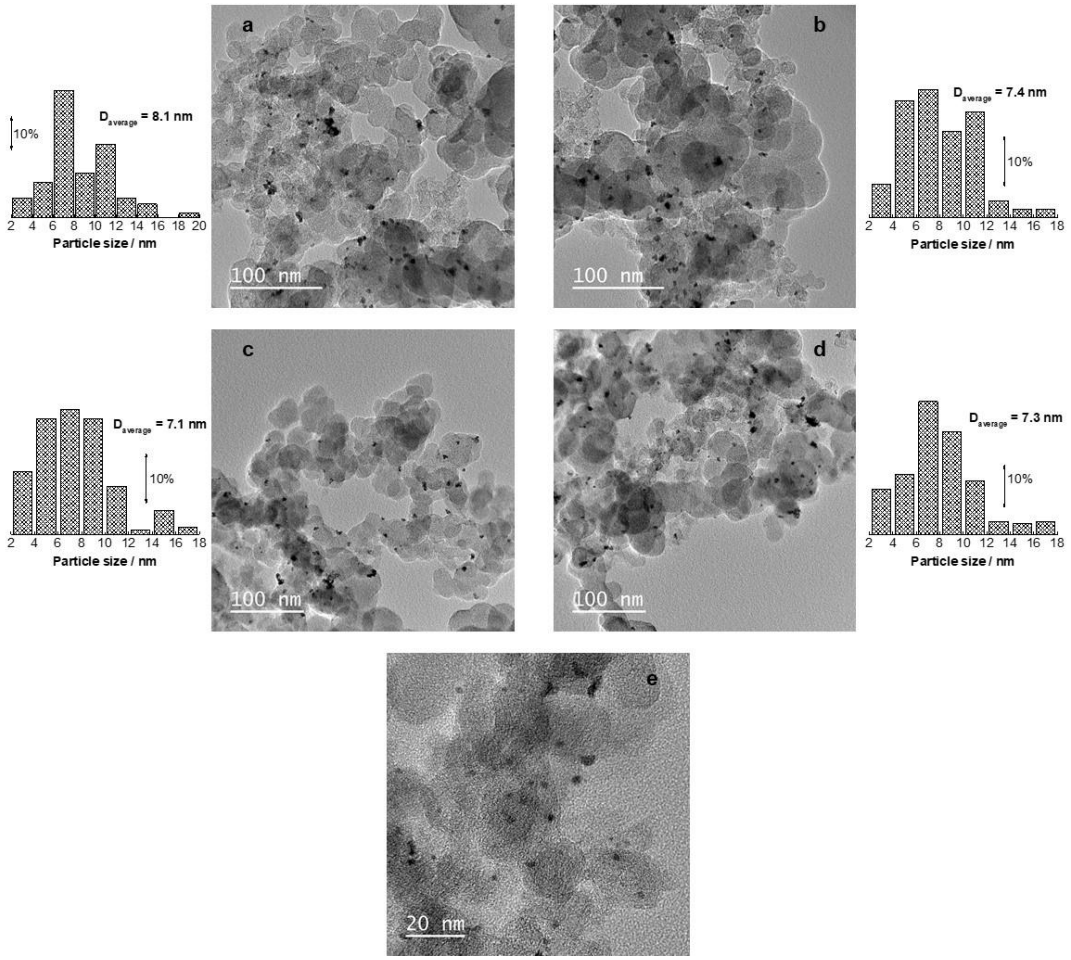

Figure 2. TEM images of the electrocatalysts: a) Pt/C, b) $Pt_{73}Cu_{27}$/C, c) $Pt_{53}Cu_{47}$/C, and d) $Pt_{29}Cu_{71}$/C and e) high-resolution image of the $Pt_{53}Cu_{57}$/C

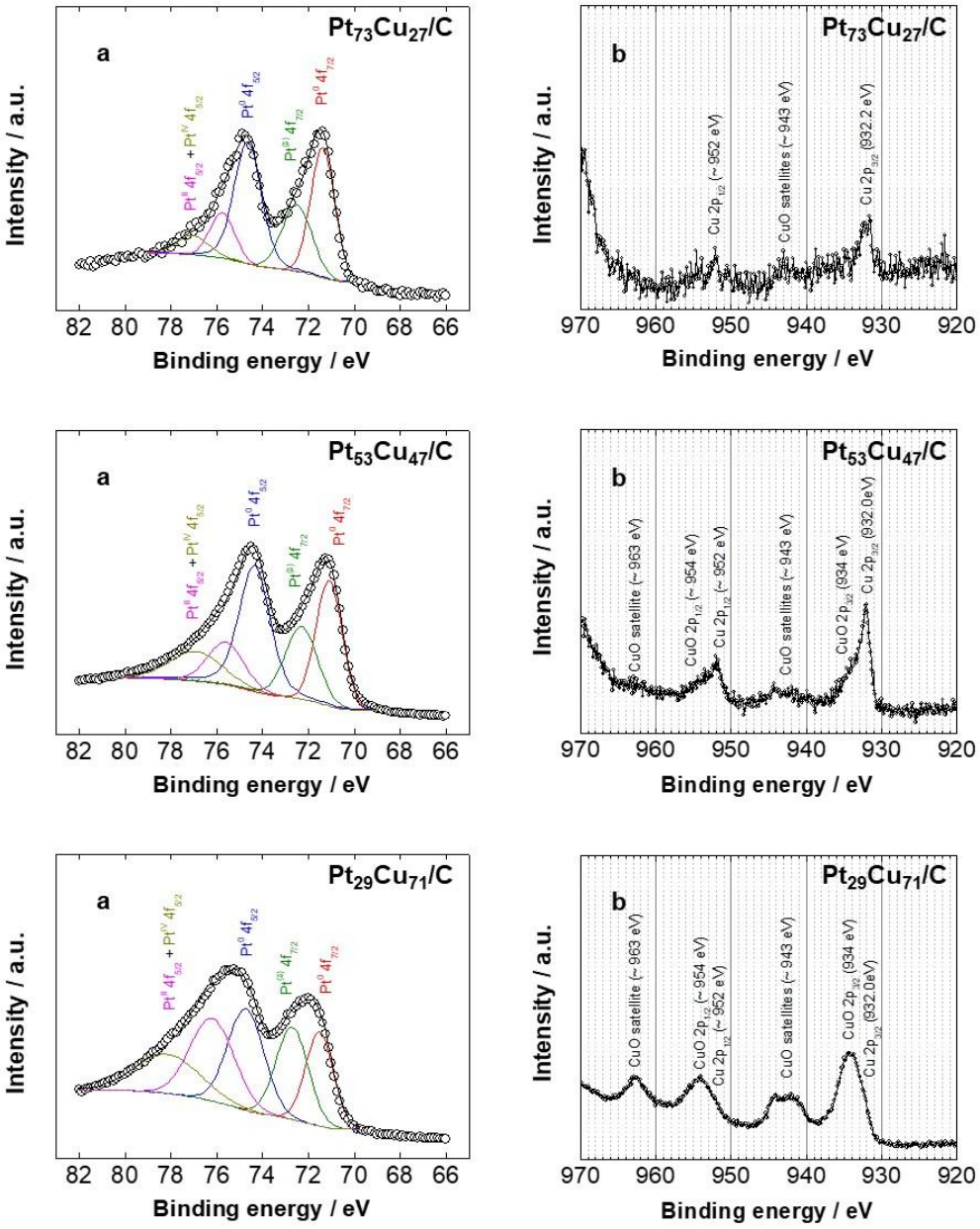

Figure 3. Pt 4*f* (a) and Cu 2*p* (b) XPS spectra of the different electrocatalysts

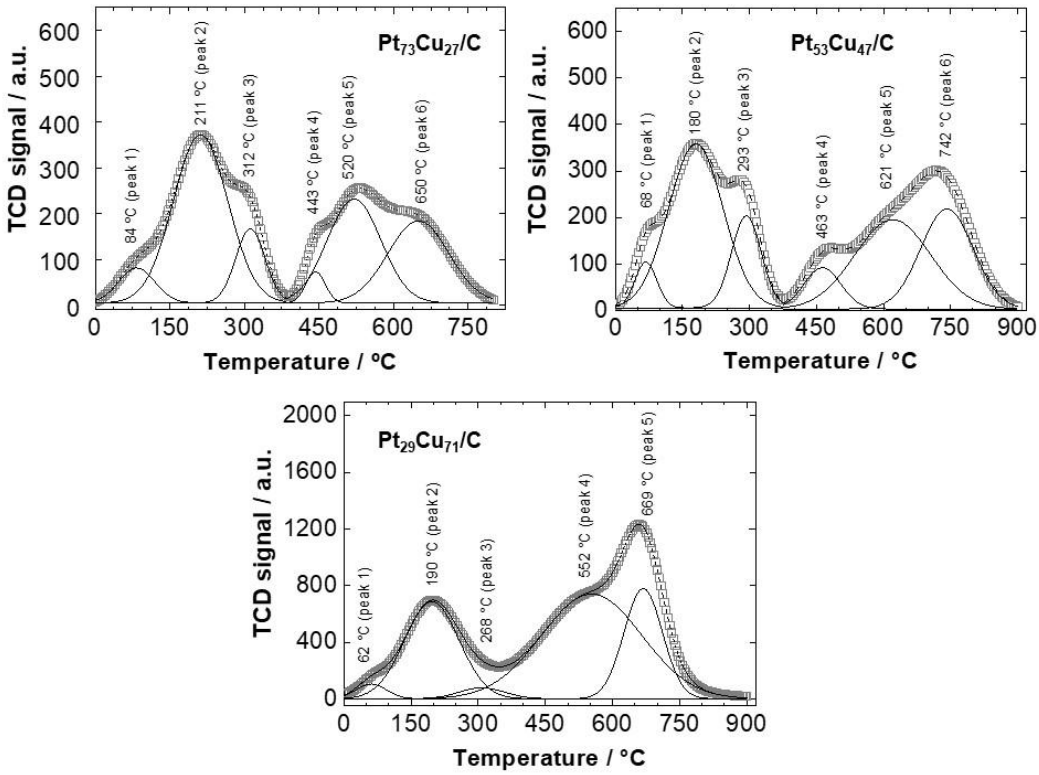

Figure 4. TPR profiles of the different bimetallic electrocatalysts prepared

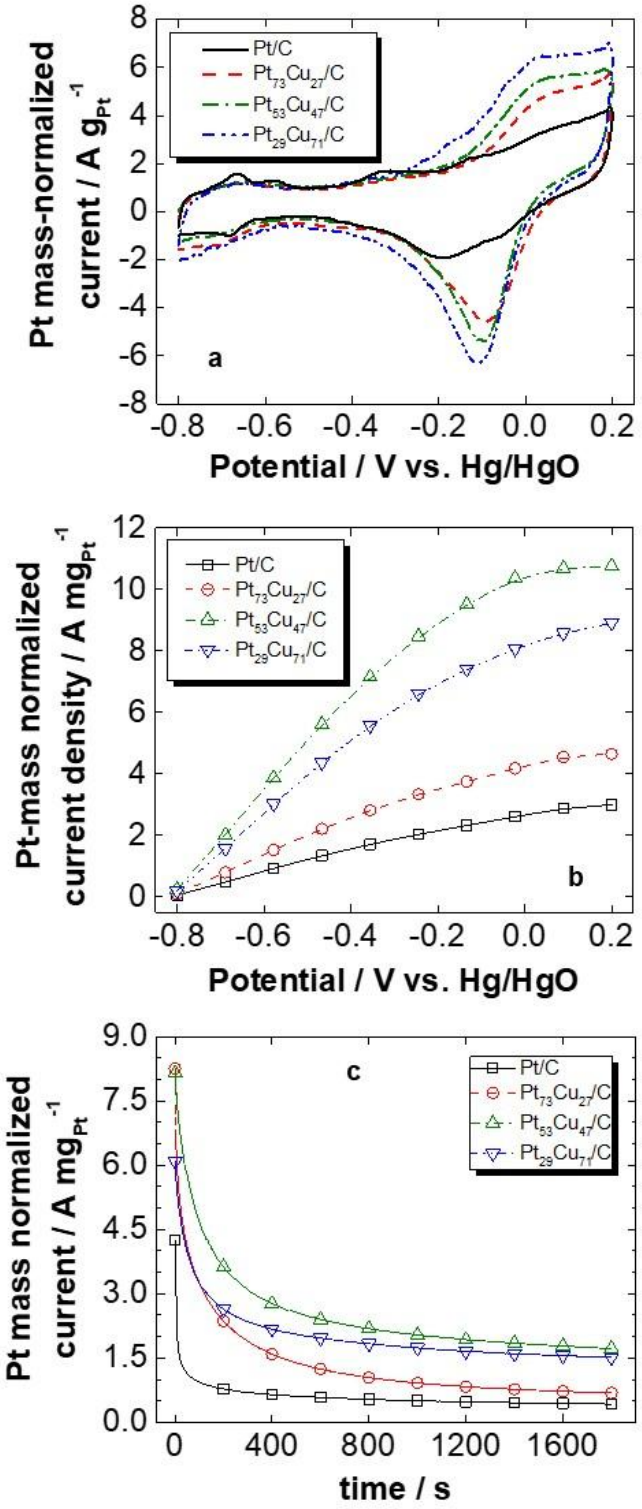

Figure 5. a) Cyclic voltammograms of the different electrocatalysts in 1 mol L^{-1} KOH; b) linear sweep voltammograms in 1 mol L^{-1} KOH and 1 mol L^{-1} hydrazine hydrate; and c) chronoamperograms at 0.024 V vs Hg/HgO in 1 mol L^{-1} KOH and 1 mol L^{-1} hydrazine hydrate

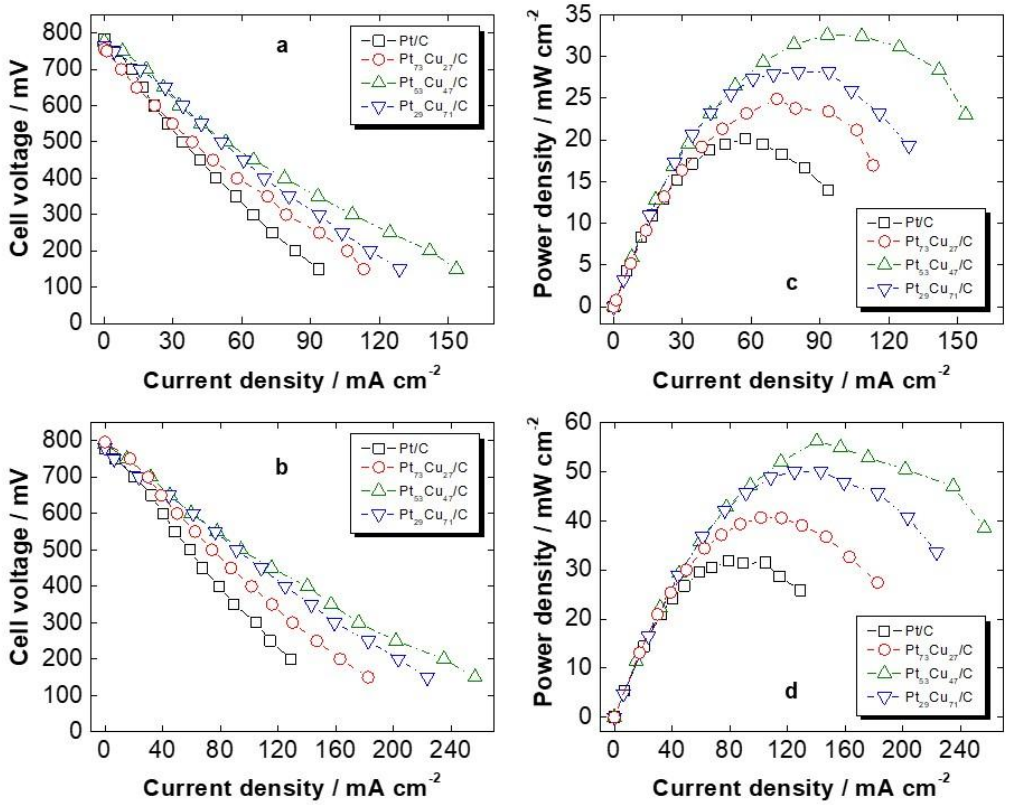

Figure 6. Polarization curves at: a) 60 ºC and b) 80 ºC; power density curves at c) 60 ºC and d) 80 ºC for the different electrocatalysts

Table 1. Pt:Cu atomic ratios for PtCu/C electrocatalysts and weight percentages of metal and carbon loadings for PtCu/C and Pt/C electrocatalysts obtained by EDX.

Electrocatalyst	Carbon loading (wt.%)	Metal loading (wt.%)	**Pt:Cu atomic ratio**	
			Nominal	**EDX**
Pt/C	80	20	–	–
$Pt_{73}Cu_{27}$/C	79	21	75:25	73:27
$Pt_{53}Cu_{47}$/C	82	18	50:50	53:47
$Pt_{29}Cu_{71}$/C	84	16	25:75	29:71

Table 2. Average crystallite sizes and lattice parameters of Pt/C and PtCu/C electrocatalysts obtained by XRD and average particle size obtained from TEM images

Electrocatalyst	Crystallite size (nm)	Lattice parameter (nm)	Cu fraction in the alloy	Fraction of Cu alloyed	Average particle size (nm)
Pt/C	4.6	0.391	–	–	8.1
$Pt_{73}Cu_{27}$/C	2.1	0.387	0.174	0.427	7.4
$Pt_{53}Cu_{47}$/C	2.3	0.382	0.337	0.428	7.1
$Pt_{29}Cu_{71}$/C	2.5	0.386	0.207	0.107	7.3

Table 3. Surface elemental analysis results for PtCu/C electrocatalysts based on XPS data.

Electrocatalyst	Atomic percentage (%)		Platinum oxidation state (%)	
	Pt	Cu	Pt (0)	Pt (δ+)
$Pt_{73}Cu_{27}/C$	77	23	56	44
$Pt_{53}Cu_{47}/C$	60	40	57	43
$Pt_{29}Cu_{71}/C$	41	59	44	56

Table 4. Maximum power density (MPD) values obtained from the power density curves in a single DHFC operating at 60 and 80 °C for Pt/C and PtCu/C electrocatalysts and percentage variation of the MPD of the PtCu/C electrocatalysts in relation to the Pt/C.

Electrocatalyst	DHFC at 60 °C		DHFC at 80 °C	
	MPD (mW cm^{-2})	PI	MPD (mW cm^{-2})	PI
Pt/C	20.1	–	31.5	–
$Pt_{73}Cu_{27}$/C	24.9	23.4	40.7	29.2
$Pt_{53}Cu_{47}$/C	32.6	62.2	56.1	78.1
$Pt_{29}Cu_{71}$/C	28.2	40.3	50.1	59.0